European Journal of Medicinal Chemistry 213 (2021) 113154

Contents lists available at ScienceDirect

European Journal of Medicinal Chemistry

journal homepage: http://www.elsevier.com/locate/ejmech

Research paper

Design, synthesis, and biological evaluation of novel xanthone-alkylbenzylamine hybrids as multifunctional agents for the treatment of Alzheimer's disease

Zhipeng Zhang [a], Jie Guo [a], Maojun Cheng [a], Weixin Zhou [a], Yang Wan [a], Rikang Wang [a], Yuanying Fang [a], Yi Jin [a], Jing Liu [b, **], Sai-Sai Xie [a, *]

[a] National Pharmaceutical Engineering Center for Solid Preparation in Chinese Herbal Medicine, Jiangxi University of Traditional Chinese Medicine, Nanchang, 330006, PR China
[b] School of Pharmacy, Jiangxi University of Traditional Chinese Medicine, Nanchang, 330006, PR China

ARTICLE INFO

Article history:
Received 4 November 2020
Received in revised form
15 December 2020
Accepted 31 December 2020
Available online 11 January 2021

Keywords:
Alzheimer's disease
Xanthone
Cholinesterase
Antioxidant
Metal chelator

ABSTRACT

In this study, a series of multifunctional hybrids against Alzheimer's disease were designed and obtained by conjugating the pharmacophores of xanthone and alkylbenzylamine through the alkyl linker. Biological activity results demonstrated that compound **4j** was the most potent and balanced dual ChEs inhibitor with IC_{50} values 0.85 μM and 0.59 μM for eeAChE and eqBuChE, respectively. Kinetic analysis and docking study indicated that compound **4j** was a mixed-type inhibitor for both AChE and BuChE. Additionally, it exhibited good abilities to penetrate BBB, scavenge free radicals (4.6 trolox equivalent) and selectively chelate with Cu^{2+} and Al^{3+} at a 1:1.4 ligand/metal molar ratio. Importantly, after assessments of cytotoxic and acute toxicity, we found compound **4j** could improve memory function of scopolamine-induced amnesia mice. Hence, the compound **4j** can be considered as a promising lead compound for further investigation in the treatment of AD.

1. Introduction

Alzheimer's disease (AD), one of the most severe and prevalent neurodegenerative diseases, affects approximately 46 million people worldwide and incurs a huge economic loss on families and societies [1]. According to the World Alzheimer Report, the population of AD will be increased up to 66 million by 2030 and 115 million by 2050 [2]. Clinical evidence demonstrate that AD is a complex disease characterized by progressive memory loss, severe behavioral abnormalities, cognitive impairment and ultimately death. Although the etiology of AD is not completely known, several factors including deficits of acetylcholine (ACh), β-amyloid (Aβ) deposits, oxidative stress, dyshomeostasis of biometals and neuroinflammation, have been appointed to play crucial roles in AD onset and progression [3].

The cholinergic hypothesis proposes that the degeneration of cholinergic neurons and the associated loss of cholinergic neurotransmission in the cerebral cortex are responsible for the deterioration of cognitive function observed in the brain of AD patients [4]. Acetylcholinesterase (AChE) and butyrylcholinesterase (BuChE) are the two types of cholinesterases (ChEs) for hydrosis of ACh in brain. The enzymatic cavity of AChE is characterized by a nearly 20 Å deep narrow gorge, which is composed of two binding sites: the catalytic active site (CAS) at the bottom and the peripheral anionic site (PAS) near the entrance of the gorge [5]. BuChE also has a similar structure of the cavity. However, compared to the BuChE, the AChE accounts for approximately 80% of ACh hydrolysis in normal brains, so it has received much attention in past decades, and many approved drugs are AChE inhibitors [6]. Additionally, apart from the function of hydrolysis of ACh, studies show that AChE can accelerate amyloid fibril formation through its peripheral anionic site (PAS), producing stable AChE-Aβ complexes, which have more neurotoxicity than single Aβ peptide [7]. Thus, dual binding site inhibitors that interact with both CAS and PAS appear to be more beneficial for AD treatment. Recent years, inhibition of BuChE is also becoming the focus on AD treatment, because a growing body of evidence has indicated that, with disease

* Corresponding author.
** Corresponding author.
E-mail addresses: liujing860828@163.com (J. Liu), xiesaisainanchang@hotmail.com (S.-S. Xie).

https://doi.org/10.1016/j.ejmech.2021.113154
0223-5234/

progression, the activity of AChE decreases to 10–15% of normal values in certain brain regions, while BuChE as a compensating enzyme is maintained at the normal or even higher level [8]. Hence, designing ChE inhibitors that simultaneously block both AChE and BuChE may lead to additional benefits for the treatment of AD.

Oxidative stress is put as one of the most important causes of Alzheimer's Disease [9]. Reactive oxygen species (ROS) including superoxide anion radical ($O_2^{\bullet -}$), hydroxyl radical (•OH) and peroxide (O_2^{2-}), and reactive nitrogen species (RNS) including peroxynitrite anion ($ONOO^-$) and nitric oxide (NO•) are primary oxidants [10]. Under normal physiological conditions, the level of oxidants formation is in equilibrium with the antioxidant capacity, while the production of oxidants overwhelms the cellular antioxidant capacity in AD [11]. The excessive generation of ROS damage the biological molecules, such as DNA, proteins and lipids, leading to the death of neurons. Therefore, engaging in accelerating the free radical scavenging is beneficial for the prevention of AD.

Metal ions are one of the necessary substances for all organisms and play an irreplaceable physiological role in the metabolic process of organisms, but high levels of biometal ions are closely implicated in the pathogenesis of AD [12]. Studies have found that the level of Cu^{2+}, Zn^{2+}, Fe^{3+}, Al^{3+} and other metal ions in the senile plaques in the brains of AD patients is higher than the background concentration of metal ions in the brains of normal people [13]. Furthermore, it was reported that the redox-active metal ions, like Cu^{2+}, interact with Aβ to produce ROS through Fenton-like reactions, thus leading to the oxidative stress and ultimately neuronal death [14]. Studies also have demonstrated that excessive Al^{3+} could not only inhibit AChE non-competitively, promote the formation of neurofibrillary tangles but also damage the dynamic balance of serum metal ions and facilitate oxidative stress, thereby triggering AD [15]. Accordingly, adjustment of such biometals in the brain may be also a promising strategy for treating AD.

Up to now, only four AChE inhibitors (rivastigmine, galantamine, donepezil, tacrine) have been approved by the US Food and Drug Administration (FDA) for the treatment of AD in clinic. However, they can only provide temporary and incomplete symptomatic relief. Considering the multifactorial pathogenesis of AD as mentioned above, we focused on multifunctional agents, which could simultaneously inhibit ChEs, chelate metals and exert antioxidant effect.

Natural products play a highly significant role in drug discovery and development processes. Xanthone (Fig. 1), chemical name is dibenzo-γ-pyrone, has been reported to display the abilities of anticancer, antibacteria, antioxidant and antineuroinflammation [16]. Recently, it was reported that xanthone derivatives could effectively inhibit AChE, and some xanthone derivatives also presented other biological activities related to AD, such as free radicals scavenging and metal ions chelation [17]. Therefore, it is advisable to design multifunctional molecules on basis of the xanthone scaffold. On the other hand, alkylbenzylamine is a versatile pharmacophore with a wide range of biological activity profiles [18]. In recent years, it has been intensively exploited to design ChE inhibitors and has been viewed as the key fragment for ChE inhibition [19]. Given the fact above, in present study, we attempted to connect xanthone with alkylbenzylamine through different length of the carbon chain linker to design novel multifunctional compounds for the treatment of AD (Fig. 1). The xanthone was utilized to interact with the PAS of AChE and entrance cavity of BuChE. Meanwhile, a hydroxyl was introduced to its 1-position, which could form intramolecular hydrogen bond with 9-carbonyl in a manner of stable six-member ring, thereby producing the abilities of scavenging free radicals and chelating metal ions. The alkylbenzylamine was employed to bind to CAS of AChE and acyl binding pocket of BuChE, which ensured that the designed compounds could inhibit both AChE and BuChE simultaneously. Furthermore, in order to get optimal linker length for balanced inhibition of AChE and BuChE, compounds with varied linker length were synthesized firstly. And once the optimal length was determined, various alkylbenzylamine groups were changed for SAR studies.

Here, a series of novel hybrids assembled by the xanthone and alkylbenzylamine fragments were synthesized and evaluated for their biological activity, including inhibition of cholinesterases, antioxidant and metal chelating effects, and the ability to cross the blood-brain barrier.

2. Results and discussion

2.1. Chemistry

The synthetic scheme for the synthesis of the compounds **4a-n** and **5a-f** are shown in Schemes 1 and 2. Initially, condensation of hydroxybenzoic acid with phloroglucinol in the presence of anhydrous zinc chloride and phosphoryl chloride afforded 1,3-dihydroxy-9H-xanthen-9-one (**2**). Considering the 1-hydroxyl of compound **2** may form intramolecular hydrogen bond with 9-carbonyl in a manner of stable six-member ring, it is less reactive in alkylation than 3-hydroxyl [20]. Thus, 3-hydroxyl group of compound **2** was directly bromoalkylated in the presence of potassium carbonate to lead to a series of 1-hydroxy-3-O-bromoalkylxanthones (**3a-f**, n = 3–8). Then, the compounds **3a-f** were reacted with corresponding secondary amines to give the target compounds **4a-n**. Finally, to further extent the structure-activity relationships, **4j** and **4n** were also selected to treat with the corresponding isocyanate to produce the additional target compounds **5a-f**.

2.2. In vitro AChE and BuChE inhibitory activity

The inhibitory activities of all synthesized hybrids towards electric eel acetylcholinesterase (AChE) and equine serum butyrylcholinesterase (BuChE) were evaluated using modified Ellman's method [21]. Inhibitory potencies are reported in Table 1 as IC_{50} (μM) or, for poorly active compounds, as the percentage of inhibition at 100 μM. As can be seen, most of the target compounds showed both AChE and BuChE inhibitory potency with IC_{50} values ranging from submicromolar to micromolar. Of these compounds, compounds **4j** and **4n** exhibited the most potent inhibitory activity for AChE (IC_{50} = 0.85 ± 0.043 μM, 0.75 ± 0.07 μM, respectively), and compounds **4e**, **4h** and **4j** showed the most potent inhibitory activity for BuChE (IC_{50} = 0.50 ± 0.005 μM, 0.79 ± 0.08 μM, 0.59 ± 0.007 μM, respectively).

To investigate the influence of the length of the carbon chain linker (n = 3–8) between the xanthone and the benzylamine moiety, compounds **4a-l** were prepared. In general, the derivatives with a three-carbon atom linker showed weak enzyme inhibition. For example, compound **4a** (AChE inhibitory activity: IC_{50} = 59.85 ± 0.14 μM) and **4g** (AChE inhibition rate at 100 μM: 34.30 ± 0.021%; BuChE inhibitory activity: IC_{50} = 32.26 ± 0.11 μM) both performed poor inhibitory activities. Elongation of the spacer to four methylene groups as seen for compounds **4b** and **4h** led to a significant increase of inhibitory potency. For example, compared with **4a** (n = 3), the AChE inhibitory activity of **4b** (n = 4) increased by about 8.8-fold (IC_{50} = 6.79 ± 0.09 μM), and compared with **4g** (n = 3), the BuChE inhibitory activity of **4h** (n = 4) increased by almost 41-fold (IC_{50} = 0.79 ± 0.08 μM).

When the linker length was extended from four to seven carbon atoms, although the tendency of the inhibitory potency was not obvious, compounds containing the linker length with even number of carbon atoms seemed better than the corresponding

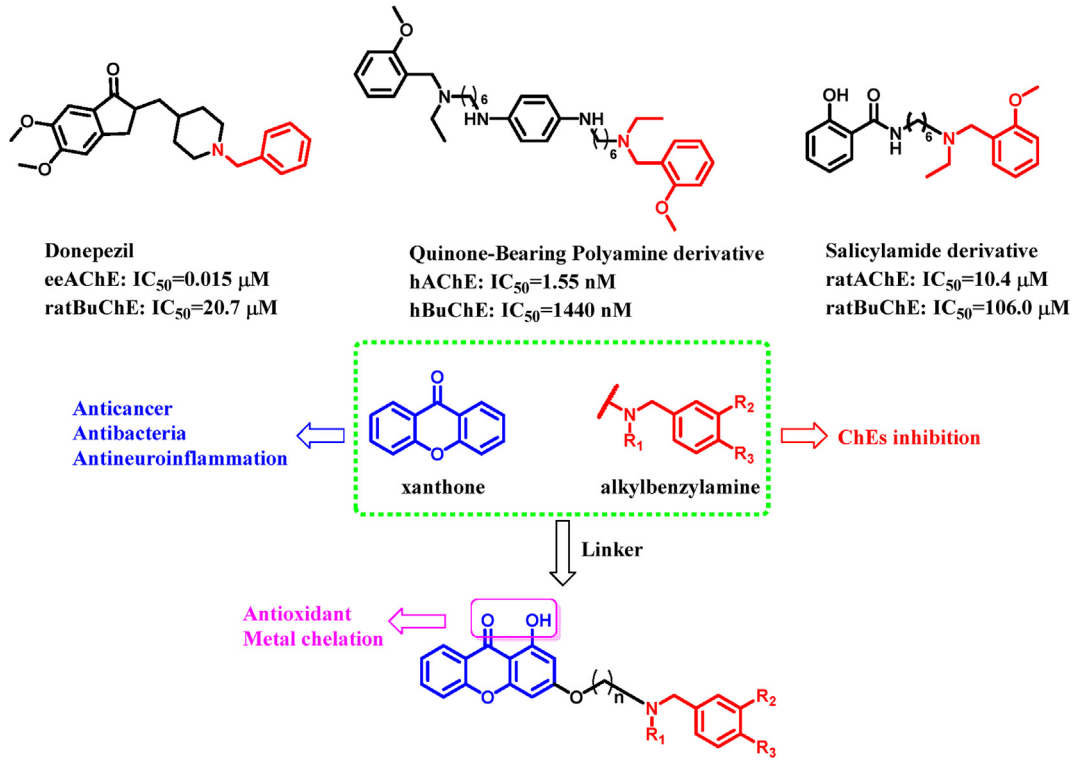

Fig. 1. Design strategy of the xanthone derivatives.

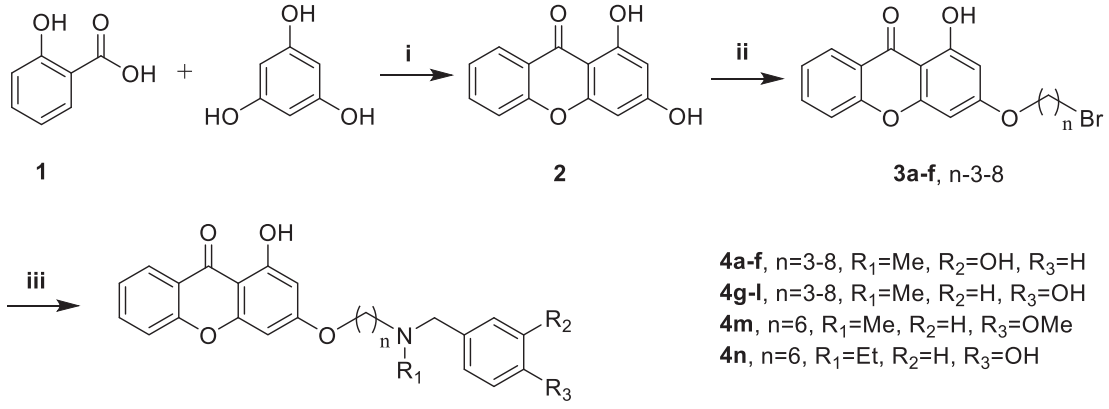

Scheme 1. Synthesis of xanthone derivatives **4a-n**. Reagents and conditions: (i) $ZnCl_2/POCl_3$, Salicylic acid, 1,3,5-trihydroxybenzene, 75 °C, 2 h; (ii) $Br(CH_2)_nBr$, K_2CO_3, DMF, r.t., 6 h; (iii) For **4a-f**: 3-((methylamino)methyl)phenol, CH_3CN, NaI, TEA, reflux, 9 h; for **4g-l**: 4-((methylamino)methyl)phenol, CH_3CN, NaI, TEA, reflux, 10 h; for **4m**: 4-Methoxy-N-methylbenzylamine, CH_3CN, NaI, TEA, reflux, 9 h; for **4n**: 4-((ethylamino)methyl)phenol, CH_3CN, NaI, TEA, reflux, 12 h.

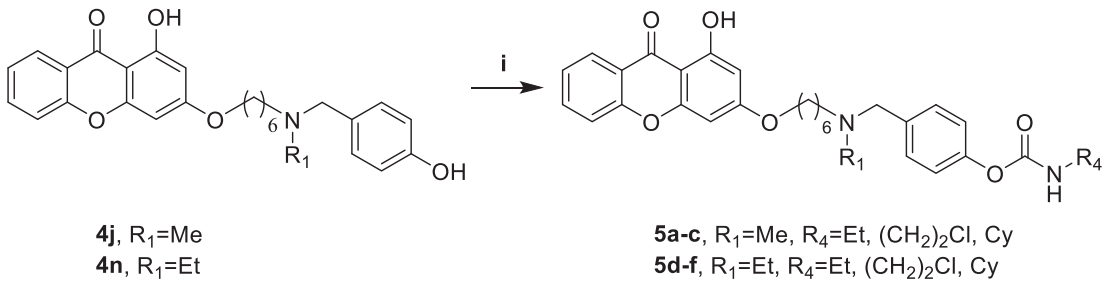

Scheme 2. Synthesis of xanthone derivatives **5a-f**. Reagents and conditions: (i) DMF, RNCO, TEA, N_2 atmosphere, r.t., 36–48 h.

Table 1
Inhibition of eeAChE and eqBuChE by compounds **4a-n** and **5a-f**.

Compd.	n	R_1	R_2	R_3	R_4	IC_{50} (μM) or inhibition rate % (100 μM)	
						eeAChE[a]	eqBuChE[b]
4a	3	Me	OH	H	–	59.85 ± 0.14	2.96 ± 0.07
4b	4	Me	OH	H	–	6.79 ± 0.09	8.94 ± 0.09
4c	5	Me	OH	H	–	80.79 ± 0.18	24.24 ± 0.14
4d	6	Me	OH	H	–	2.68 ± 0.10	22.33 ± 0.12
4e	7	Me	OH	H	–	8.24 ± 0.06	0.50 ± 0.005
4f	8	Me	OH	H	–	42.60 ± 0.017%	6.14 ± 0.02
4g	3	Me	H	OH	–	34.30 ± 0.021%	32.26 ± 0.11
4h	4	Me	H	OH	–	1.79 ± 0.08	0.79 ± 0.08
4i	5	Me	H	OH	–	1.60 ± 0.12	3.87 ± 0.04
4j	6	Me	H	OH	–	0.85 ± 0.043	0.59 ± 0.007
4k	7	Me	H	OH	–	7.43 ± 0.03	1.82 ± 0.08
4l	8	Me	H	OH	–	42.60 ± 0.015%	9.53 ± 0.05
4m	6	Me	H	OMe	–	55.02 ± 0.17	9.37 ± 0.06
4n	6	Et	H	OH	–	0.75 ± 0.07	1.70 ± 0.09
5a	6	Me	H	–	Et	9.69 ± 0.15	24.00 ± 0.74%
5b	6	Me	H	–	$(CH_2)_2Cl$	1.02 ± 0.21	1.74 ± 0.14
5c	6	Me	H	–	Cy	141.9 ± 0.22	40.10 ± 0.21%
5d	6	Et	H	–	Et	2.41 ± 0.04	1.15 ± 0.13
5e	6	Et	H	–	$(CH_2)_2Cl$	1.90 ± 0.05	1.03 ± 0.04
5f	6	Et	H	–	Cy	22.23 ± 0.13	1.15 ± 0.03

[a] AChE from electric eel (EeAChE). All values are expressed as mean ± SD from three independent experiments.
[b] BuChE from equine serum (eqBuChE). All values are expressed as mean ± SD from three independent experiments.

compounds containing the linker length with odd number of carbon atoms (AChE inhibitory activity: **4b** (n = 4) > **4c** (n = 5), **4d** (n = 6) > **4e** (n = 7), **4j** (n = 6) > **4k** (n = 7); BuChE inhibitory activity: **4b** (n = 4) > **4c** (n = 5), **4h** (n = 4) > **4i** (n = 5), **4j** (n = 6) > **4k** (n = 7)). Further elongating the linker length to eight carbon atoms led to a sharp drop in the both ChEs inhibitory activity of all compounds. For example, the AChE inhibitory activity of **4e** (n = 7, IC_{50} = 8.24 ± 0.06 μM) and **4k** (n = 7, IC_{50} = 7.43 ± 0.03 μM) both decreased to 42.6% inhibition rate at 100 μM. The BuChE inhibitory activity of **4e** and **4k** respectively decreased by 12-fold (**4e**: IC_{50} = 0.50 ± 0.005 μM *vs* **4f**: n = 8, IC_{50} = 6.14 ± 0.02 μM) and 5.3-fold (**4k**: IC_{50} = 1.82 ± 0.08 μM *vs* **4l**: n = 8, IC_{50} = 9.53 ± 0.05 μM).

Additionally, it also revealed that the position of the substituent of the terminal benzene ring affected the activities. Most of compounds **4g-l** possessing a hydroxyl substituent at 4-position of the benzene ring usually displayed better activities than corresponding those **4a-f** with a hydroxyl substituent at 3-position (AChE inhibitory activity: **4h** > **4b**, **4i** > **4c**, **4j** > **4d**, **4k** > **4e**; BuChE inhibitory activity: **4h** > **4b**, **4i** > **4c**, **4j** > **4d**). Among them, compound **4j**, bearing a hydroxyl group at 4-position of the terminal benzene ring and a six-methylene linker, exhibited the optimal and balanced inhibition activity against ChEs. Therefore, we decided to select **4j** for further optimation.

Compounds **4m** and **4n** were obtained by modification at benzylamine moiety in **4j** for exploring the SARs. Noticeably, compared with compound **4j**, when maintaining the methyl group at R_1, the installation of a methoxy group at 4-position of the benzene ring dramatically decreased AChE and BuChE inhibitory activity, which made the IC_{50} values change from 0.85 μM to 55.02 μM (**4m**) for AChE and 0.59 μM to 9.37 μM (**4m**) for BuChE. In contrast, when maintaining the hydroxyl group at R_3, the introduction of an ethyl group at R_1 slightly enhanced the AChE inhibitory activity (**4n**: IC_{50} = 0.75 ± 0.07 μM), but reduced BuChE inhibitory activity (**4n**: IC_{50} = 1.70 ± 0.09 μM).

According to the previous studies, the carbamate group tend to be transferred onto the serine-OH in the CAS, which enhances the binding affinity between the target compound and enzyme [22]. Thus, a series of new compounds **5a-f** were synthesized. Unfortunately, the activities against AChE and BuChE were not improved, but reduced. In general, compounds possessing N-ethyl substitution at R_1 were more active than those with N-methyl substitution, and compounds containing the chloroethyl (**5b**, **5e**) at R_4 performed relatively better than those with the ethyl and cyclohexyl substitutions, which suggested that electron-withdrawing effect of chlorine atom might be positive.

Above all, the results demonstrated that compound **4j** was the most optimal compound as a dual inhibition agent for AChE and BuChE, which implied the H-bond effect between the terminal hydroxyl and CAS of ChEs was required.

2.3. In vitro antioxidant activity assay

Free radicals-induced oxidative stress is believed to be conducive to the progression of AD [23]. Thus, each compound was preliminarily determined for scavenging activity by the DPPH (diphenyl-1-picrylhydrazyl) radical scavenging method and ABTS (2, 2′-azino-bis(3-ethylbenzthiazoline-6-sulfonicacid)) radical scavenging method [24,25]. Trolox, a water-soluble vitamin E analog, was used as a reference standard. From Table 2, it could be seen that the range of the variation of the free radicals scavenging activity is wide. Among these compounds, although less potent than trolox, compound **4c** exhibited the most potent activity. In general, the length of methylene chain affected the antioxidant activities. For example, the abilities of compounds **4a-f** and **4g-l** (n = 3, 4, 5, 6, 7, 8) to capture free radicals were decreased as the length of the alkyl chain were increased. Moreover, the position of the hydroxyl group of the terminal benzene ring also affected the activity. The compounds (**4a-f**) with the hydroxyl group at 3-position showed more effective activities than compounds (**4g-l**) with that at 4-position, which was opposite with the ChEs inhibitory abilities. Strikingly, replacement of the hydroxyl group on the terminal benzene ring by other groups, affording compounds **5a-f**, led to an obvious decline in potency of scavenging the DPPH and ABTS free radicals.

The oxygen radical absorbance capacity assay (ORAC-FL) was also performed to evaluate the antioxidant activity of each compound. As shown in Table 2, the tested compounds displayed poor to excellent antioxidant abilities that expressed as a trolox equivalent. Among them, compounds **4a-d**, **4h**, **4j**, **4n**, **5e** exhibited the excellent free radical quenching abilities (ORAC > 1). Especially compound **4b** (ORAC = 6.11) exerted optimal radical scavenging activity and is close to the well-known strong free radical scavenging agent, quercetin (ORAC = 6.55). Similarly, the structure-activity relationships obtained by the ORAC method were basically consistent with the trend from DPPH and ABTS methods. However, compound **4b**, rather than **4c**, presented the most potent antioxidant activity determined by the ORAC method, which may probably be attributed to the fact that DPPH and ABTS are both in fact a kind of nitrogen radicals while AAPH is the peroxyl radical inducer [26].

2.4. In vitro blood-brain barrier permeation assay

Blood-brain barrier (BBB) permeability is the major requirement for drugs acting at targets inside of the central nervous system [27]. Thus, the parallel artificial membrane permeability assay was performed to predict the BBB permeation of the target compounds [28,29]. First, the permeabilities of 9 commercial drugs with their reported values were used to validate the assay in Table 3. And a plot of experimental data *versus* the bibliographic values gave a good linear correlation: P_e (exp.) = 0.6703 × P_e (bibl.) + 0.6571 (R^2 = 0.9623). It could be seen from the Table 4 that, with exception

Table 2
DPPH and ABTS scavenging activities and Oxygen Radical Absorbance Capacity by Fluorescence (ORAC-FL, Trolox Equiv) of the synthesized compounds.

Compd.	n	R_1	R_2	R_3	R_4	IC_{50} (μM) or inhibition (%)		ORAC[c]
						DPPH[a]	ABTS[b]	
4a	3	Me	OH	H	–	31.4 ± 0.52%	46.95 ± 0.63	4.78 ± 0.08
4b	4	Me	OH	H	–	521.9 ± 0.72	32.48 ± 0.55	6.11 ± 0.12
4c	5	Me	OH	H	–	456.9 ± 0.68	30.25 ± 0.48	1.04 ± 0.04
4d	6	Me	OH	H	–	708.2 ± 0.77	32.04 ± 0.50	2.39 ± 0.03
4e	7	Me	OH	H	–	719 ± 0.69	52.68 ± 0.61	0.42 ± 0.01
4f	8	Me	OH	H	–	2387 ± 0.96	34.57 ± 0.49	0.035 ± 0.01
4g	3	Me	H	OH	–	544.9 ± 0.80	56.45 ± 0.65	0.79 ± 0.02
4h	4	Me	H	OH	–	648.7 ± 0.81	66.97 ± 0.68	3.34 ± 0.05
4i	5	Me	H	OH	–	1074 ± 0.93	33.52 ± 0.32	0.44 ± 0.02
4j	6	Me	H	OH	–	1280 ± 0.92	41.64 ± 0.33	4.60 ± 0.09
4k	7	Me	H	OH	–	1306 ± 0.85	20.94 ± 0.25%	0.05 ± 0.01
4l	8	Me	H	OH	–	1751 ± 0.87	33.75 ± 0.41	<0.01
4m	6	Me	H	OMe	–	25.9 ± 0.29%	58.77 ± 0.55	<0.01
4n	6	Et	H	OH	–	25.6 ± 0.30%	60.10 ± 0.58	1.69 ± 0.07
5a	6	Me	H	–	Et	36.8 ± 0.44%	33.89 ± 0.41%	0.26 ± 0.03
5b	6	Me	H	–	$(CH_2)_2Cl$	35.1 ± 0.43%	37.98 ± 0.47%	0.43 ± 0.02
5c	6	Me	H	–	Cy	48.9 ± 0.53%	14.51 ± 0.16%	0.093 ± 0.01
5d	6	Et	H	–	Et	23.3 ± 0.26%	27.61 ± 0.27%	0.92 ± 0.04
5e	6	Et	H	–	$(CH_2)_2Cl$	33.4 ± 0.43%	70.60 ± 0.67	2.31 ± 0.08
5f	6	Et	H	–	Cy	40.3 ± 0.51%	41.00 ± 0.35	0.35 ± 0.02
Trolox						15.5 ± 0.13	13.8 ± 0.14	–
Quercetin						–	–	6.55 ± 0.11

[a] The 50% inhibitory concentration of DPPH or percent inhibition with inhibitor at 1 mM (means ± SD of three experiments).
[b] The 50% inhibitory concentration of ABTS or percent inhibition with inhibitor at 100 μM (means ± SD of three experiments).
[c] Data are expressed as μM of Trolox equivalent/μM of tested compound and are mean (n = 3) ± SD.

of the compounds **4f** and **5b**, which exhibited questionable BBB permeability (CNS±), most of the target compounds have P_e values above the threshold ($P_e = 3.33 \times 10^{-6}$ cm/s), indicating that they have great BBB permeability (CNS+) and enough drug exposure in the central nervous system.

2.5. Kinetic study of the AChE and BuChE inhibitions by compound *4j*

To better understanding of the inhibition mechanism, kinetic studies of compound **4j** as a dual AChE and BuChE inhibitor were performed. As shown in Fig. 2**A** and **C**, the Lineweaver-Burk double reciprocal plots revealed increasing slopes (decreased V_{max}) and intercepts (higher K_m) with higher inhibitor concentrations and intersected in the second quadrant. This pattern indicated that **4j** was a mixed-type inhibitor for both AChE and BuChE. Replots of the slope *versus* concentrations were utilized to obtain the inhibition constants (K_i), which were estimated to be 1.4 μM and 0.98 μM for AChE and BuChE respectively based on Fig. 2**B** and **D**.

Table 3
Permeability p_e ($\times 10^{-6}$ cm/s) in the PAMPA-BBB assay for 9 commercial drugs in the experiment validation.

Commercial drugs	Bibliography[a]	Experiment[b]
Testosterone	17.0	10.86 ± 0.46
Estradiol	12.0	9.38 ± 0.35
Progesterone	9.3	7.53 ± 0.25
Chlorpromazine	6.5	6.20 ± 0.12
Caffeine	1.3	1.33 ± 0.03
Corticosterone	5.1	4.06 ± 0.05
Hydrocortisone	1.9	1.71 ± 0.11
Atenolol	0.8	0.22 ± 0.02
Theophylline	0.1	0.83 ± 0.05

[a] Taken from Ref. [30].
[b] Experimental data are expressed as mean ± SD from three independent experiments, using PBS: EtOH (70:30) as solvent.

2.6. Molecular docking of AChE and BuChE by *4j*

To gain insight into the interaction of compound **4j** with the active site residues of AChE and BuChE, a computational study was performed using the docking program by the X-ray crystal structures of *hu*AChE (PDB code: 4EY7), *ee*AChE (PDB code: 2CKM) and *hu*BuChE (PDB code: 1P0I).

In the *hu*AChE-**4j** complex, compound **4j** occupied the entire *hu*AChE enzymatic catalytic site (CAS), the mid-gorge site and the

Table 4
Permeability P_e ($\times 10^{-6}$ cm/s) in the PAMPA-BBB assay for all compounds and their predicted penetration into CNS.

Compd.	P_e ($\times 10^{-6}$ cm/s)[a]	predictoin[b]
4a	6.09 ± 0.33	CNS+
4b	12.87 ± 0.62	CNS+
4c	11.03 ± 0.55	CNS+
4d	15.17 ± 0.48	CNS+
4e	9.27 ± 0.19	CNS+
4f	3.20 ± 0.12	CNS±
4g	11.94 ± 0.23	CNS+
4h	16.91 ± 0.33	CNS+
4i	11.50 ± 0.45	CNS+
4j	5.29 ± 0.21	CNS+
4k	4.39 ± 0.13	CNS+
4l	10.03 ± 0.17	CNS+
4m	6.82 ± 0.15	CNS+
4n	5.95 ± 0.14	CNS+
5a	5.09 ± 0.09	CNS+
5b	2.33 ± 0.11	CNS±
5c	4.61 ± 0.12	CNS+
5d	7.38 ± 0.36	CNS+
5e	5.02 ± 0.21	CNS+
5f	7.36 ± 0.18	CNS+

[a] Experimental data are expressed as mean ± SD from three independent experiments, using PBS: EtOH (70:30) as solvent.
[b] Compounds with permeabilities $P_e > 3.33 \times 10^{-6}$ cm/s could cross the BBB by passive diffusion (CNS+). Compounds with $P_e < 2.00 \times 10^{-6}$ cm/s could not cross the BBB (CNS -), and compounds with 2.00×10^{-6} cm/s $< P_e < 3.33 \times 10^{-6}$ cm/s indicate uncertain BBB permeation (CNS±).

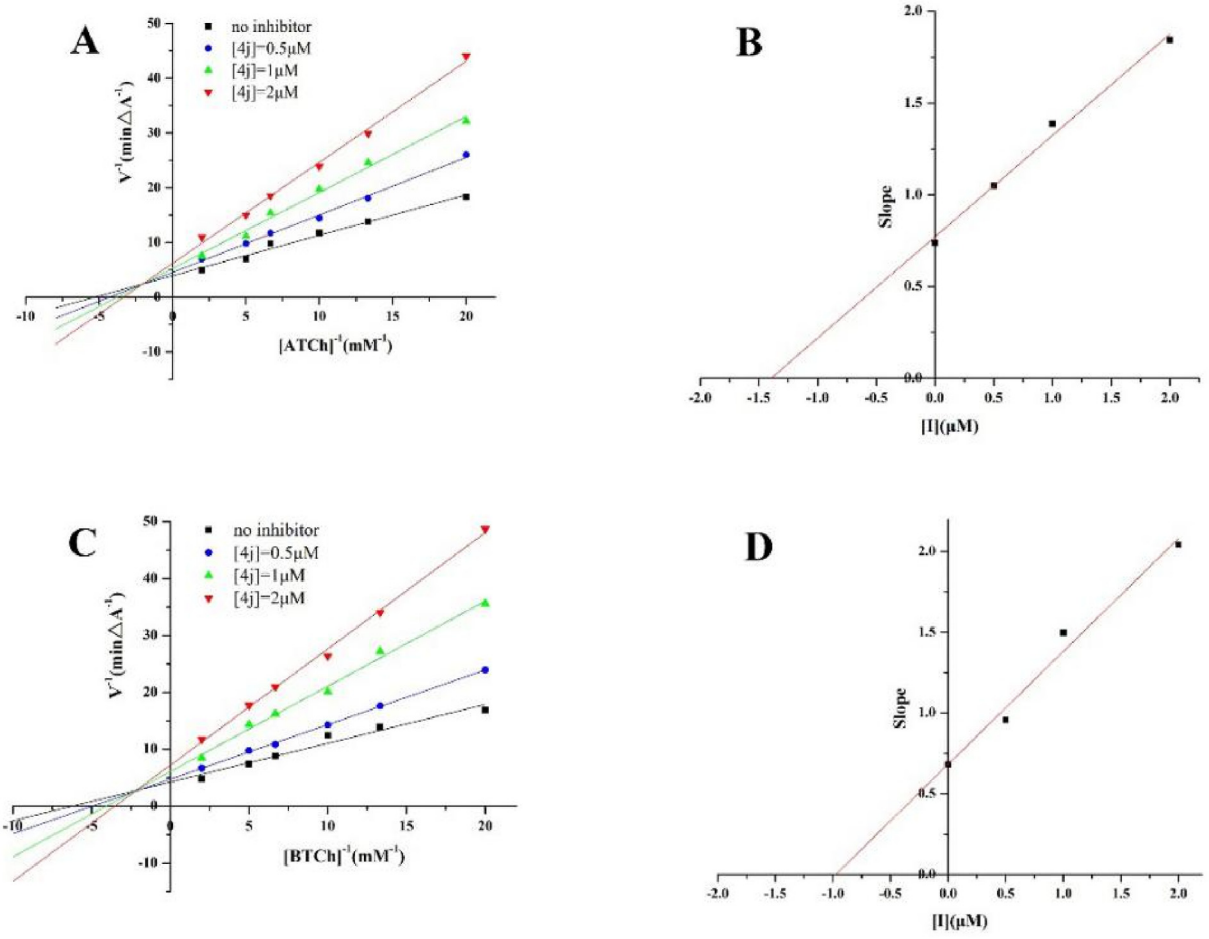

Fig. 2. Lineweaver-Burk plot of **4j** for AChE hydrolysis (A) and slope replot *vs* **4j** concentration (B). Lineweaver-Burk plot of **4j** for BuChE hydrolysis (C) and slope replot *vs* **4j** concentration (D).

peripheral anionic site (PAS) (Fig. 3**A** and **C**). The xanthone moiety of **4j** was oriented towards the PAS of *hu*AChE, *via* a face-to-face aromatic π-π stacking interaction between its phenyl ring and the indole ring from Trp286 at PAS. Besides, the carbonyl oxygen of xanthone moiety generated a hydrogen bond with the Arg296, which further enhanced the binding ability to PAS. The flexible alkylene linker extended the alkylbenzylamine deep into CAS of *hu*AChE through aromatic π-π stacking interactions with the phenyl ring from Trp86. Moreover, the hydroxyl group of the alkylbenzylamine formed a hydrogen bond with Glu202 at the anionic subsite. Also, compound **4j** was modeled into the structure of *ee*AChE (Fig. 3**B** and **D**). The docking pose of compound **4j** in the *ee*AChE was similar to that in the *hu*AChE. The xanthone moiety of **4j** interacted with the Trp279 and Tyr70 at PAS of *ee*AChE and the alkylbenzylamine of **4j** interacted with the Trp84 and Glu199 at CAS of *ee*AChE, which was broadly in line with the results in *hu*AChE.

The AChE and BuChE share more than 50% homological amino acid sequences [31,32]. Despite the similarity between two enzymes, the presence of a similar PAS in BuChE is still under discussion [22]. In contrast to the aromatic amino acids forming the PAS in AChE, several relatively small aliphatic amino acids endow BuChE with a wider pocket in the comparable area of BuChE, whereas only Asp70 and Tyr332 are conserved.

In the *hu*BuChE-**4j** complex, xanthone, the bulkier moiety of **4j**, located near the entrance cavity of *hu*BuChE (Fig. 4**A** and **B**). This pose was stabilized by a π-π stacking interaction between two phenyl rings respectively from the xanthone and Tyr332. In the middle gorge, the alkylene linker folded in a conformation in gorge that provided optimum flexibility to the terminal phenyl group to insert deep within the active-site gorge. The terminal benzene ring and its hydroxyl group bound to Trp231 and Leu286 of the acyl binding pocket (Trp 231, Leu 286, Val 288) at the bottom of the gorge *via* π-π interactions and hydrogen bond respectively [33]. In addition, the charged nitrogen of alkylbenzylamine interacted with His438 residue of the catalytic triad (Ser 198, Glu 325, His 438) *via* cation-π interaction, which is pivotal for *hu*BuChE inhibition [34].

The observed docking studies between the ligand and residues provided the reasonable explain for mixed-type inhibition model of kinetic studies, which agreed with the dual binding site mode.

2.7. Metal-chelating properties

Research showed that the fragment of 2-hydroxyl and 9-carbonyl group in the xanthone, which can form intramolecular hydrogen bond in a manner of stable six-member ring, is responsible for the metal chelation ability. Based on the above studies, we selected the compound **4j** as representative to investigate its abilities to chelate biometals such as Na^{+}, Mg^{2+}, Fe^{2+}, Zn^{2+}, Ca^{2+}, Al^{3+} and Cu^{2+}, using UV−vis and fluorescence spectroscopy. As shown in Fig. 5**A**, the specific fluorescence emission peak of **4j** can be observed at 300 nm ($\lambda_{ex} = 232$ nm). After NaCl, $MgCl_2$, $FeCl_2$, $ZnCl_2$ and $CaCl_2$ were added to the solution of **4j**, the fluorescence

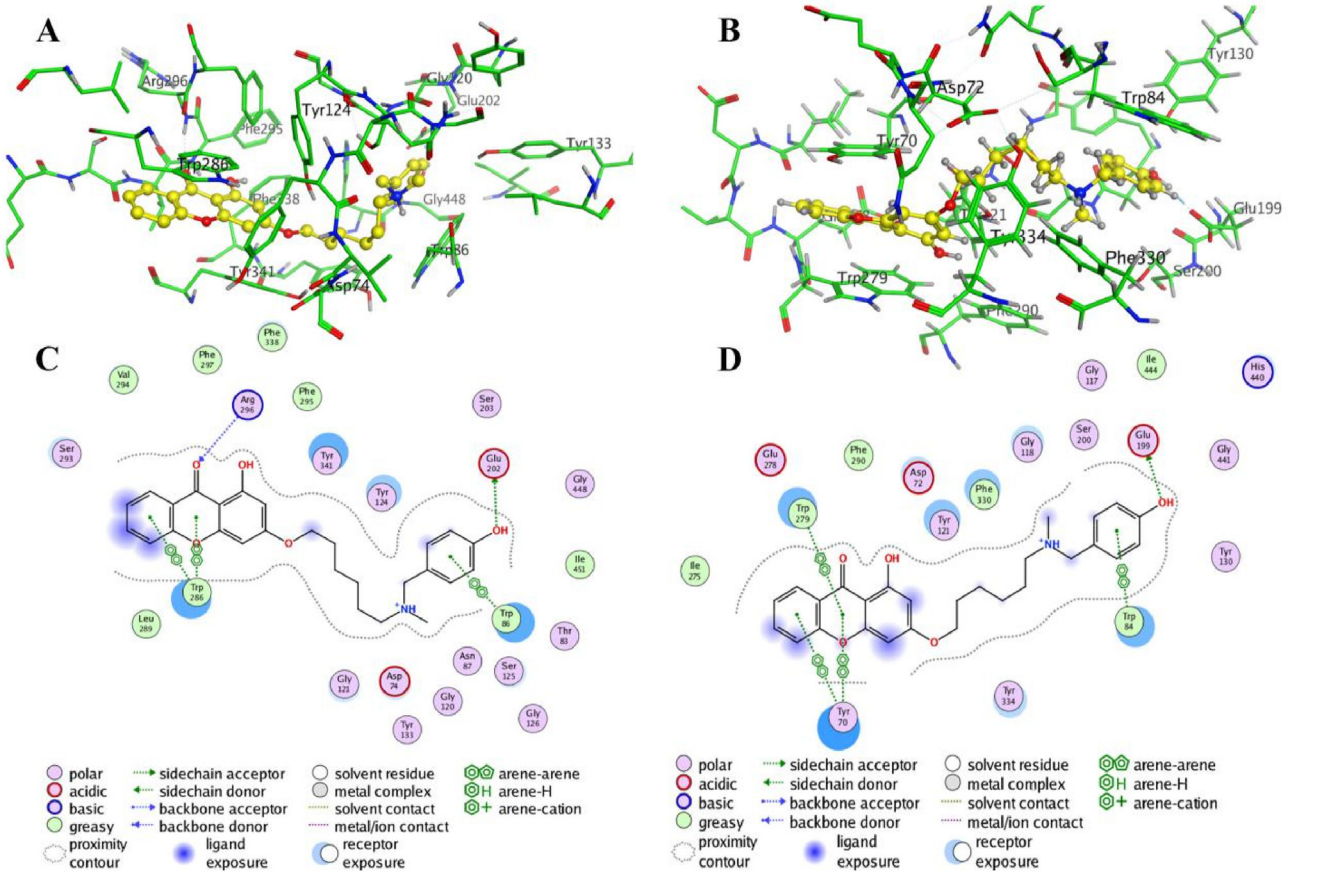

Fig. 3. Molecule docking results: A) and C) were 3D and 2D docking models of compound **4j** (yellow stick) with *hu*AChE (PDB code: 4EY7) complex generated with MOE; B) and D) were 3D and 2D docking models of compound **4j** (yellow stick) with *ee*AChE (PDB code: 2CKM) complex generated with MOE. (For interpretation of the references to color in this figure legend, the reader is referred to the Web version of this article.)

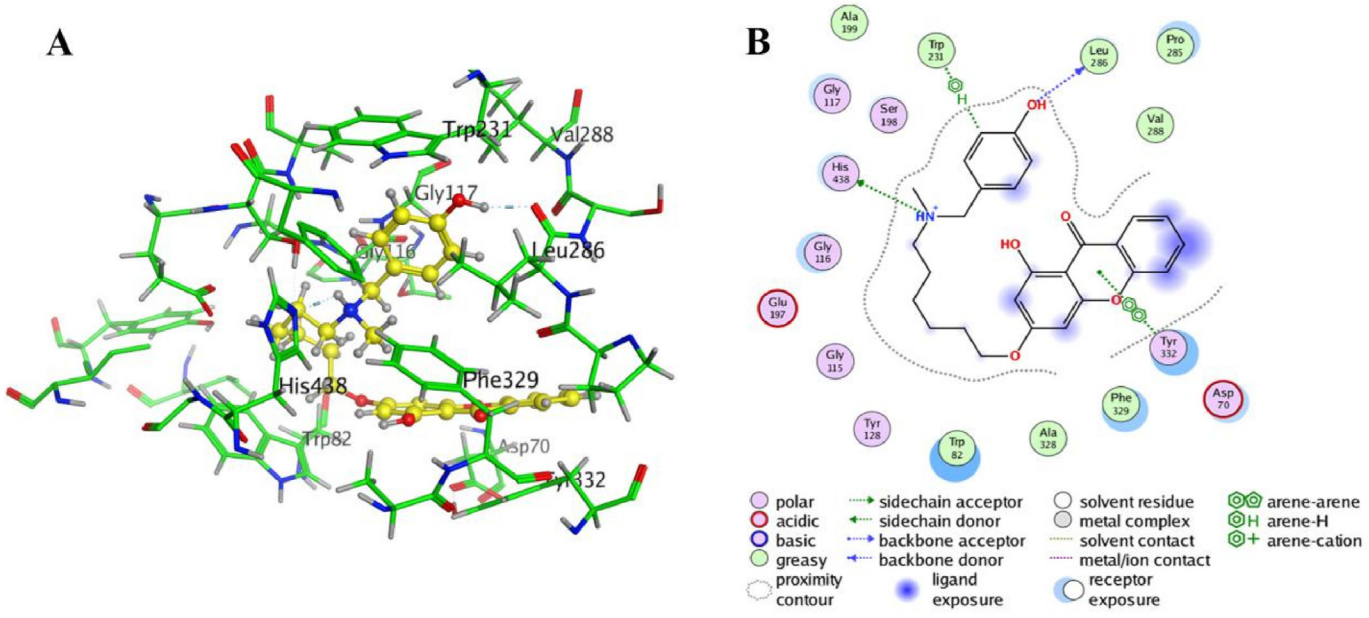

Fig. 4. Molecule docking results: A) and B) were 3D and 2D docking models of compound **4j** (yellow stick) with *hu*BuChE (PDB code: 1P0I) complex generated with MOE. (For interpretation of the references to color in this figure legend, the reader is referred to the Web version of this article.)

intensity of the emission peaks decreased variously, while the fluorescence intensity obviously increased with the addition of $AlCl_3$ and $CuCl_2$. These phenomena are indicative of a possible interaction between these biometals and ligand. Also, a UV–vis

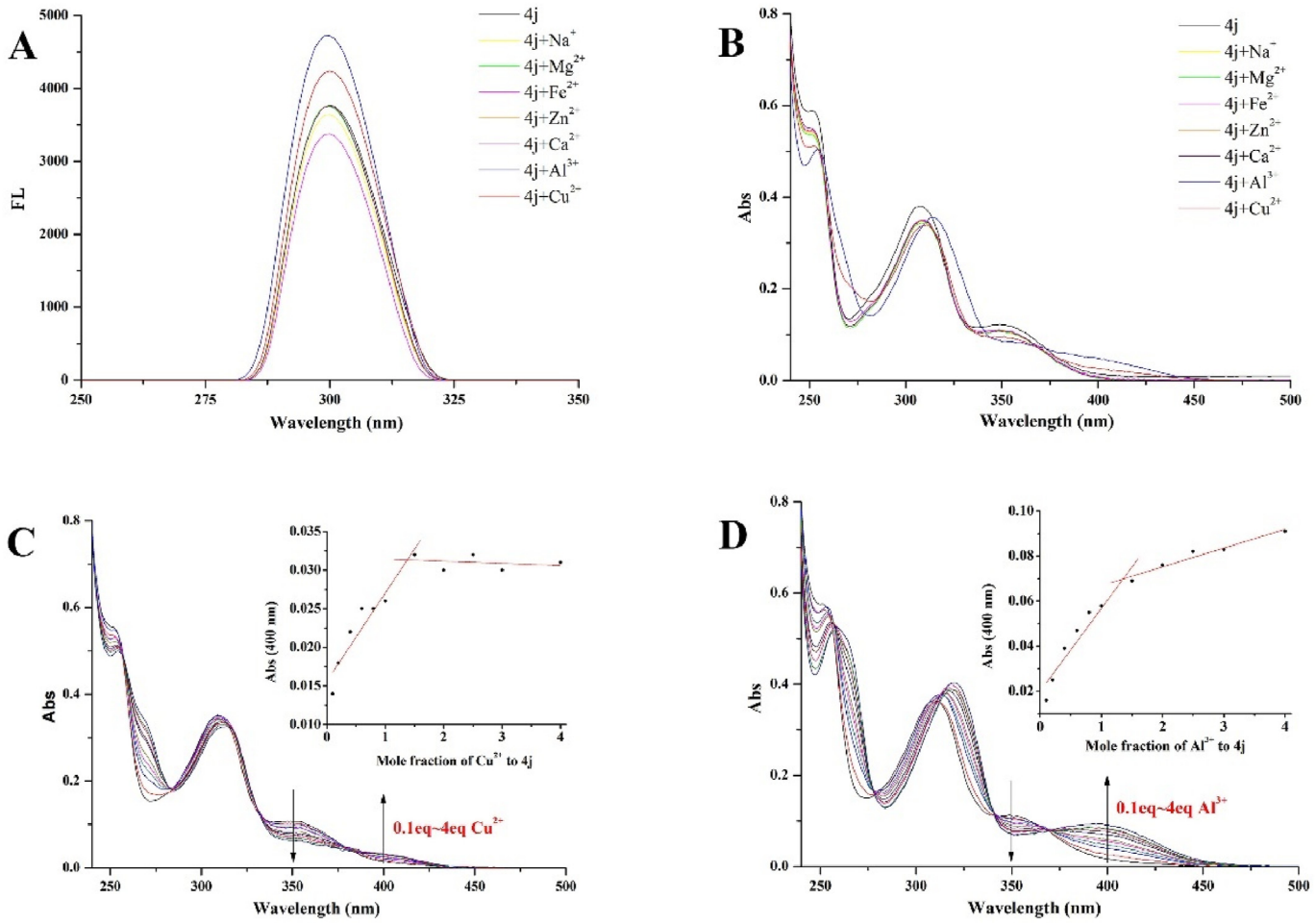

Fig. 5. (A) Fluorescence spectra of **4j** (50 μM in methanol/water) alone or in the presence of NaCl, $MgCl_2$, $FeCl_2$, $ZnCl_2$, $CaCl_2$, $AlCl_3$ and $CuCl_2$ (1 equivalent in methanol/water). (B) UV absorbance spectra of **4j** (50uM in methanol/water) alone or in the presence of NaCl, $MgCl_2$, $FeCl_2$, $ZnCl_2$, $CaCl_2$, $AlCl_3$ and $CuCl_2$(1 equivalent in methanol/water). (C) Determination of the stoichiometry of the **4j**-Cu^{2+} complex by the molar ratio method. (D) Determination of the stoichiometry of the **4j**-Al^{3+} complex by the molar ratio method.

spectroscopy assay was performed to further evaluate the metal-chelating properties of **4j**. As shown in Fig. 5**B**, the absorption peak at the original 308 nm shift to 315 nm with the intensity decreasing moderately and the spectra trough at the 270 nm moved to 283 nm after the addition of $AlCl_3$. Meanwhile, new optical band was detected at approximately 400 nm. Similarly, when $CuCl_2$ was added, a red shift from 270 nm to 283 nm with the intensity increasing significantly and new optical band was also detected at approximately 400 nm. There were only vague optical shift and slight fluctuation of maximum absorption peak after the addition of the other biometals. These results demonstrated that compound **4j** could selectively chelate with Cu^{2+} and Al^{3+}. To further confirm the metal-chelating properties of **4j**, the stoichiometries of the **4j**-Cu^{2+} and **4j**-Al^{3+} complexes were determined using molar ratio method. Following the absorption at 400 nm, a series of UV−vis spectra were collected of **4j** titrated with ascending amounts of $CuCl_2$ and $AlCl_3$ respectively as shown in Fig. 5**C** and **D**. It can be seen from the embedded figures, the absorbance linearly increased initially and then became stable. For the **4j**-Cu^{2+} and **4j**-Al^{3+} complexes, the two sets of straight lines both intersected at a 1.4:1 Cu^{2+}/ligand and Al^{3+}/ligand molar ratio.

2.8. In vitro cytotoxicity evaluation

To investigate the safety of the compound **4j**, its 5 different concentrations (6.25, 12.5, 25, 50 and 100 μM) were tested using the neural cells (PC12 and BV-2), hepatic cells (HepG2) and cardiomyocytes (H9C2) by the Cell Counting Kit-8 (CCK-8) [35]. Tacrine was used as a positive control. From the results shown in Fig. 6, **4j** did not show modified cell viability on two neural cell lines less than 12.5 μM. And the toxic dose of **4j** on cells HepG2 was higher than that of **4j** on neural cell lines, which up to the concentration of 25 μM. Although **4j** presented the more than 50% cell toxicity on cells H9C2 at 25 μM or higher concentrations, it exerted no obvious toxicity below the 12.5 μM. Therefore, compound **4j** has a medium therapeutic safety range and it is necessary to further evaluate the safety in vivo.

2.9. Acute toxicity assay

Forty KM mice (18−22 g, n = 10 per group, half male and half female) that are common closed colony mice and most widely used in biomedical research in China were randomly allocated into 4 groups [36]. The tested compound **4j** was delivered to mice by oral administration at four doses of 0, 625, 1250 and 2500 mg/kg. During the treatment period, no death and abnormal behaviors (emesis-like or diarrhea behavior) were observed and the body weights gradually enhanced (Fig. 7). Moreover, the mean body weight of the mice in the compound group presented no significant differences with those in the control group. Furthermore, all mice were sacrificed on the 14th day after drug administration, and no significant histological abnormal changes were detected in the

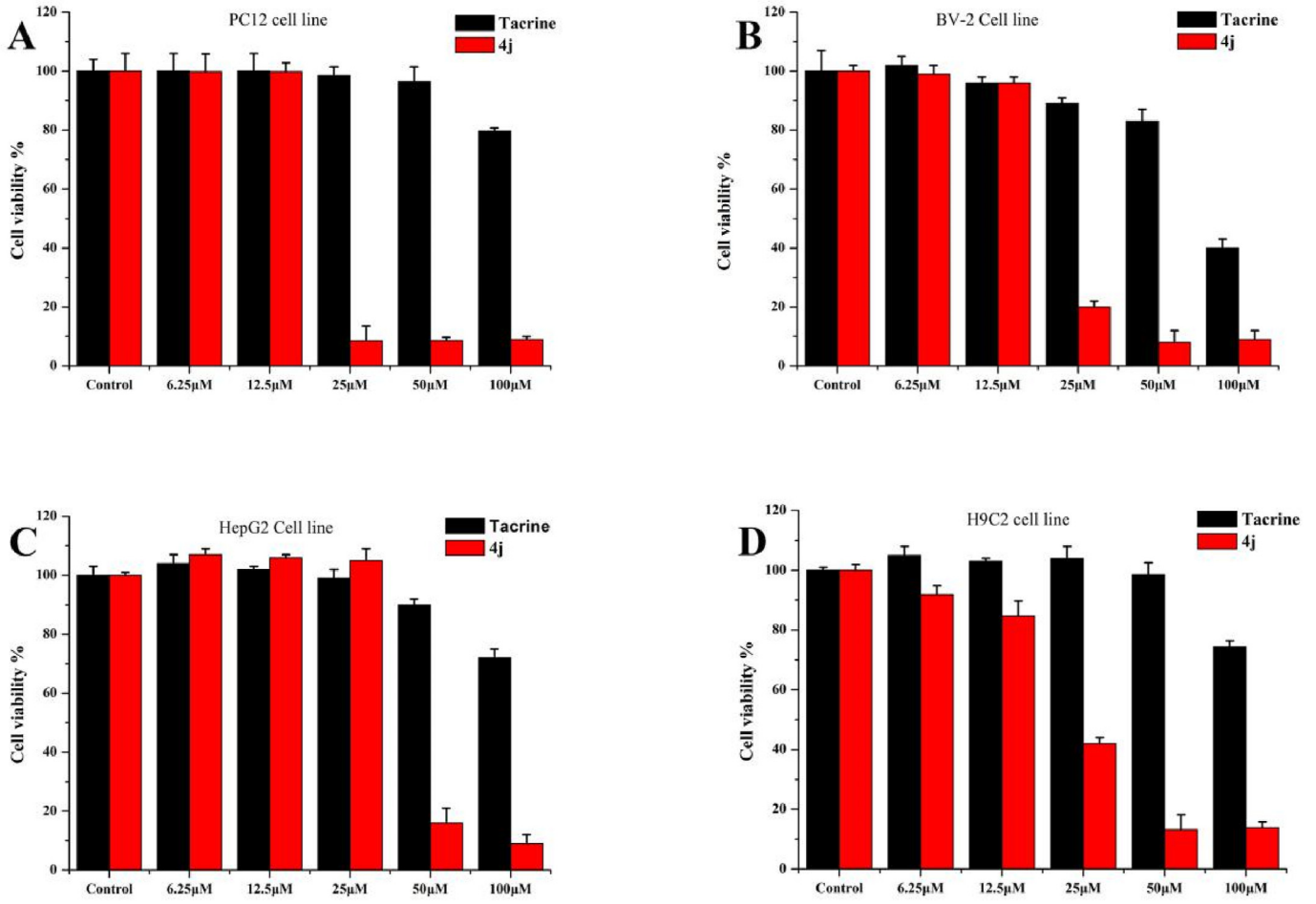

Fig. 6. Cytotoxicity of compound **4j** on neural cells (PC12 and BV-2), hepatic cells (HepG2) and cardiomyocytes (H9C2) over coincubation for 24 h. Tacrine was used as a positive control.

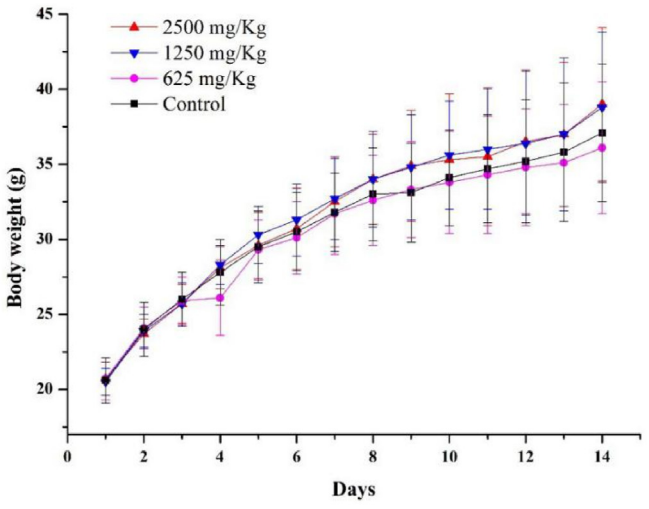

Fig. 7. The mean daily body weight profile of mice in different groups during the therapy period (n = 10).

heart, liver, lung, kidney and brain of the mice at the maximum tested dosage 2500 mg/kg by hematoxylin and eosin (HE) staining (Fig. 8) [37]. Overall, compound **4j** demonstrated no acute toxicity and was well tolerated at doses up to 2500 mg/kg.

2.10. Cognitive and memory improvement test

Considering the good ChEs inhibitory activity and safety of **4j**, we further investigated its effect on memory impairment induced by scopolamine (3 mg/kg, i.p.) in mice *via* the step-down test [38]. Donepezil (10 mg/kg) was used as a positive control. Compound **4j** and donepezil were orally administered into the KM mice 1 h before each training trial [39]. As shown in Fig. 9, compared with the control group, treatment with scopolamine led to a much shorter step-down latency time (250.7 *vs* 65.3 s, $p < 0.05$), and the number of errors was significantly increased (0.3 *vs* 2.3, $p < 0.001$), which indicated the successful establishment of the memory impairment mice model. After treatment with **4j**, the latency and number of the errors were reversed in a dose-dependent manner. Moreover, high (100 mg/kg) and medium (50 mg/kg) dose groups could prolong the step-down latency and exhibited a comparable activity to donepezil group. And high dose group showed fewer numbers of errors, but medium and low (25 mg/kg) dose groups displayed a worse effect. As a conclusion, compound **4j** improved cognitive deficit by increasing brain cholinergic level.

2.11. Theoretical prediction of the ADME properties

To investigate the drug-like profiles of **4j**, the ADME properties were estimated using SwissADME web tool. As shown in Table 5, compound **4j** fulfilled the requirements of Lipinski's and Veber's

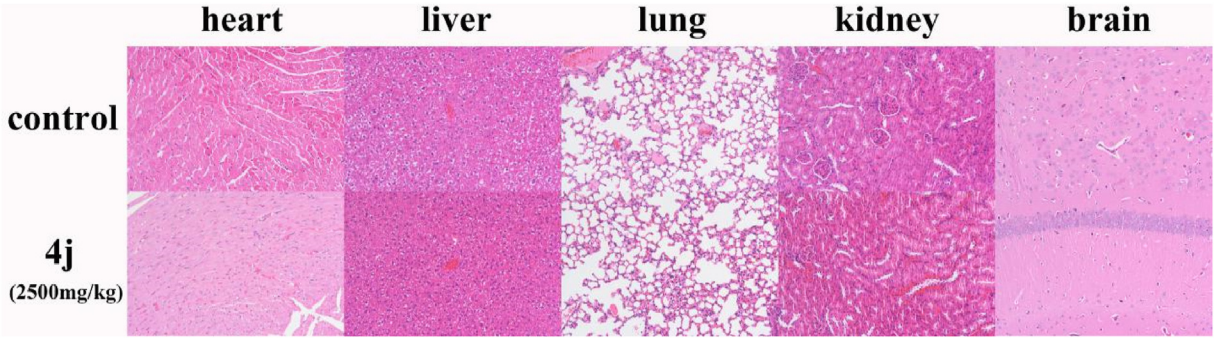

Fig. 8. Histological analysis of heart, liver, lung, kidney, and brain for the acute toxicity studies of compound **4j** at dosage of 2500 mg/kg in mice; 200 mm indicate the scale bar of images (HE staining). Representative images of HE-stained liver, heart, lung, kidney and brain for each group are shown.

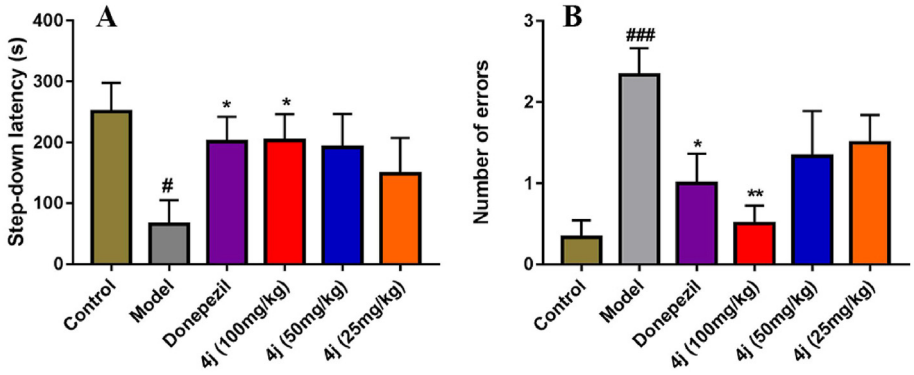

Fig. 9. Effects of compound **4j** on scopolamine-induced memory deficit in the step-down passive avoidance test. (A) latency time, (B) number of errors. Values are expressed as the mean ± SEM. n = 6 mice from three independent experiments; #p < 0.05, ###p < 0.001 versus control group; *p < 0.05, **p < 0.01 versus model group.

rules, and its structure did not contain any characteristic structural elements of pan-assay interference compounds (PAINS), suggesting that target compound **4j** presented drug-likeness properties.

3. Conclusion

In summary, a series of xanthone-alkylbenzylamine hybrids were designed, synthesized and evaluated as multifunctional agents for the treatment of Alzheimer's disease. Most of the target compounds displayed moderate to good ChEs inhibitory activities. Among them, compound **4j** exhibited both AChE and BuChE sub-micromolar inhibitory potency with IC_{50} values 0.85 μM and 0.59 μM. The kinetic analysis revealed that **4j** showed mixed-type inhibition, which was consistent with the docking studies. In addition, compound **4j** exerted significant metal-chelating ability with Cu^{2+} and Al^{3+} at a 1:1.4 ligand/Cu^{2+} and ligand/Al^{3+} molar ratio and free radicals scavenging capacity (4.6 trolox equivalent). The PAMPA assay showed that **4j** could cross the BBB and interact at targets inside of the central nervous system. To investigate the safety of the compound **4j**, we found it no acute toxicity and it was well tolerated at doses up to 2500 mg/kg. Most importantly, the step-down test showed **4j** dose-dependently reversed scopolamine-induced memory deficit. All of these results made compound **4j** a promising candidate in the development of anti-AD drugs.

Table 5
Drug-likeness properties of selected compound.

Compd.	MW[a]	nrotb[b]	nON[c]	nOHNH[d]	tPSA[e]	ilogP[f]	PAINS alerts
4j	447.52	10	6	2	83.14	4.50	0

[a] MW: molecular weight.
[b] nrotb: number of rotatable bonds.
[c] nON: number of hydrogen acceptors.
[d] nOHNH: number of hydrogen donors.
[e] tPSA: total polar surface area.
[f] ilog P: octanol/water partition coefficent.

4. Experimental section

4.1. Chemistry

All chemical reagents and solvents were purchased from commercial suppliers and used without further purification. Reaction progress was monitored by thin-layer chromatography (TLC) on silica gel GF_{254} plates from Qingdao Haiyang Chemical Co. Ltd. (China), and then visualized by UV light (254 nm). Chromatographic separation were performed on silica gel (100–200 mesh) from Qingdao Haiyang Chemical Co. Ltd. (China). Melting points were determined in glass capillary tubes on an XT-4 micro melting point apparatus (China) and are uncorrected. ^{1}H NMR spectra (600 MHz) and ^{13}C NMR spectra (151 MHz) were recorded on a Bruker ACF-600 spectrometer at room temperature using $CDCl_3$ or DMSO-d_6 as the solvent. Chemical shifts (δ) are reported in parts per million (ppm) relative to tetramethylsilane (TMS), and spin multiplicities are given as s (singlet), d (doublet), t (triplet), m (multiplet) or br (broad). The purity of these compounds was determined by analytical HPLC performed on a Waters ACQUITY Arc HPLC system equipped with a 2998 PDA detector. (Column: Agilent XDB-C18, 5 μm particle size, 4.6 mm × 250 mm; mobile phase: A = CH_3OH, B = H_2O (0.1% acetic acid), isocratic elution, A = 75%, B = 25%; flow

rate = 1 mL/min; λ = 254 nm; 10 μL injection). All target compounds possessed purity higher than 95%. High resolution mass spectra were conducted on an AB Sciex Triple TOF 5600 spectrometer (HR-ESI-MS).

4.2. Synthesis of 1,3-dihydroxy-9H-xanthen-9-one (**2**)

To a 50-mL flask, 17 mL phosphorus oxychloride ($POCl_3$) and anhydrous zinc chloride (14.8 g, 0.11 mol) were added. The suspension was stirred at 75 °C until $ZnCl_2$ was completely dissolved into phosphorus oxychloride. Then salicylic acids (7.24 mmol) and 1,3,5-trihydroxybenzene (7.96 mmol) were added, respectively, and the mixture was heated at 75 °C for 2 h. After the mixture was cooled down to r. t., the mixture was pulled into ice water stirring for 10 min and extracted with ethyl acetate (25 mL × 3). The ethyl acetate layer was collected, dried over anhydrous sodium sulfate, filtered and concentrated under reduced pressure to give the crude product **2**. The residue was purified on a silica gel chromatography using petroleum ether/ethyl acetate (25:3 to 5:2) as eluent.

4.3. General procedure for the synthesis of (**3a-f**)

To a mixture of compound **2** (200 mg, 0.88 mmol) and anhydrous potassium carbonate (242 mg, 1.75 mmol) in DMF (5 mL), appropriate dibromoalkane derivative (22 mmol) was added. The reaction mixture was allowed to stir for 6 h at room temperature until the starting material disappeared. Then the mixture was filtered and concentrated under reduced pressure to give the crude product. The residue was purified by silica gel chromatography using petroleum ether/ethyl acetate (30:1) as eluent to afford the desired products **3a-f**.

4.3.1. 3-(3-bromopropoxy)-1-hydroxy-9H-xanthen-9-one (**3a**)

Yield 79%; yellow solid; m.p. 123–125 °C; ^{1}H NMR (600 MHz, DMSO) δ 12.80 (d, *J* = 2.4 Hz, 1H), 8.16 (dd, *J* = 7.8, 1.2 Hz, 1H), 7.90–7.87 (m, 1H), 7.62 (d, *J* = 8.4 Hz, 1H), 7.51–7.49 (m, 1H), 6.68 (d, *J* = 1.8 Hz, 1H), 6.43 (d, *J* = 2.4 Hz, 1H), 4.24 (t, *J* = 6.0 Hz, 2H), 3.68 (t, *J* = 6.6 Hz, 2H), 2.39–2.16 (m, 2H).

4.3.2. 3-(4-bromobutoxy)-1-hydroxy-9H-xanthen-9-one (**3b**)

Yield 80%; yellow solid; m.p. 118–120 °C; ^{1}H NMR (600 MHz, DMSO) δ 12.79 (s, 1H), 8.15 (dd, *J* = 7.8, 1.8 Hz, 1H), 7.90–7.87 (m, 1H), 7.61 (d, *J* = 8.4 Hz, 1H), 7.49 (d, *J* = 7.8 Hz, 1H), 6.64 (d, *J* = 2.0 Hz, 1H), 6.40 (d, *J* = 1.8 Hz, 1H), 4.17 (t, *J* = 6.0 Hz, 2H), 3.74 (t, *J* = 6.6 Hz, 2H), 2.04–1.93 (m, 2H), 1.91–1.80 (m, 2H).

4.3.3. 3-((5-bromopentyl)oxy)-1-hydroxy-9H-xanthen-9-one (**3c**)

Yield 82%; yellow solid; m.p. 124–126 °C; ^{1}H NMR (600 MHz, DMSO) δ 12.81 (s, 1H), 8.17 (d, *J* = 7.8 Hz, 1H), 7.90 (t, *J* = 7.2 Hz, 1H), 7.63 (d, *J* = 8.4 Hz, 1H), 7.51 (t, *J* = 7.2 Hz, 1H), 6.66 (s, 1H), 6.42 (s, 1H), 4.15 (t, *J* = 6.0 Hz, 2H), 3.58 (t, *J* = 6.6 Hz, 2H), 1.89 (t, *J* = 7.2 Hz, 2H), 1.79 (t, *J* = 7.2 Hz, 2H), 1.55 (t, *J* = 6.6 Hz, 2H).

4.3.4. 3-((6-bromohexyl)oxy)-1-hydroxy-9H-xanthen-9-one (**3d**)

Yield 80%; yellow solid; m.p. 134–135 °C; ^{1}H NMR (600 MHz, DMSO) δ 12.81 (s, 1H), 8.17 (d, *J* = 12.0 Hz, 1H), 7.90 (t, *J* = 6.0 Hz, 1H), 7.63 (d, *J* = 6.0 Hz, 1H), 7.51 (t, *J* = 6.0 Hz, 1H), 6.67 (s, 1H), 6.42 (s, 1H), 4.14 (t, *J* = 6.0 Hz, 2H), 3.56 (t, *J* = 6.0 Hz, 2H), 1.84 (d, *J* = 6.0 Hz, 2H), 1.76 (s, 2H), 1.46 (s, 4H).

4.3.5. 3-((7-bromoheptyl)oxy)-1-hydroxy-9H-xanthen-9-one (**3e**)

Yield 81%; yellow solid; m.p. 114–115 °C; ^{1}H NMR (600 MHz, $CDCl_3$) δ 12.88 (s, 1H), 8.27 (d, *J* = 7.8 Hz, 1H), 7.73 (t, *J* = 7.8 Hz, 1H), 7.45 (d, *J* = 8.4 Hz, 1H), 7.40 (t, *J* = 7.2 Hz, 1H), 6.44 (s, 1H), 6.36 (s, 1H), 4.07 (t, *J* = 6.0 Hz, 2H), 3.45 (t, *J* = 7.2 Hz, 2H), 1.93–1.83 (m, 4H), 1.53–1.50 (m, 4H), 1.45–1.42 (m, 2H).

4.3.6. 3-((8-bromooctyl)oxy)-1-hydroxy-9H-xanthen-9-one (**3f**)

Yield 78%; yellow solid; m.p. 99–101 °C; ^{1}H NMR (600 MHz, $CDCl_3$) δ 12.88 (s, 1H), 8.27 (dd, *J* = 7.8, 1.8 Hz, 1H), 7.75–7.72 (m, 1H), 7.45 (dd, *J* = 8.4, 0.6 Hz, 1H), 7.41–7.38 (m, 1H), 6.45 (d, *J* = 2.4 Hz, 1H), 6.36 (d, *J* = 2.4 Hz, 1H), 4.07 (t, *J* = 6.6 Hz, 2H), 3.44 (t, *J* = 6.6 Hz, 2H), 1.92–1.82 (m, 4H), 1.51–1.46 (m, 4H), 1.43–1.38 (m, 4H).

4.4. General procedure for the synthesis of 1-hydroxyl-3-aminoalkoxyxanthen derivatives (**4a-n**)

To a mixture of sodium iodide (77 mg, 0.51 mmol), appropriate intermediates **3a-f** (0.51 mmol) and the corresponding secondary amines (0.61 mmol) in acetonitrile (10 mL), triethylamine (0.77 mmol) was added. The reaction mixture was refluxed for 9–12 h. Upon completion of the reaction, the mixture was filtered when hot and concentrated under reduced pressure to give the crude product. The residue was purified by silica gel chromatography to give compounds **4a-n**, respectively.

4.4.1. 1-Hydroxy-3-(3-((3-hydroxybenzyl) (methyl)amino) propoxy)-9H-xanthen-9-one (**4a**)

It was prepared from 3-(3-bromopropoxy)-1-hydroxy-9H-xanthen-9-one (**3a**) and 3-((methylamino)methyl)phenol according to the general procedure, then purified on a silica gel chromatography eluted with dichloromethane/methanol (25:1) to obtain the pure product **4a**. 69% yield; yellow solid; m.p. 145–147 °C; ^{1}H NMR (600 MHz, DMSO) δ 12.81 (s, 1H), 9.72 (s, 1H), 8.17 (d, *J* = 7.8 Hz, 1H), 7.90 (t, *J* = 8.4 Hz, 1H), 7.63 (d, *J* = 8.4 Hz, 1H), 7.51 (t, *J* = 7.8 Hz, 1H), 7.27 (s, 1H), 6.89 (d, *J* = 28.2 Hz, 3H), 6.66 (s, 1H), 6.40 (s, 1H), 4.36 (s, 1H), 4.22 (s, 3H), 3.18 (s, 2H), 2.72 (s, 3H), 2.18 (s, 2H). ^{13}C NMR (151 MHz, DMSO) δ 180.68, 165.99, 163.08, 158.09, 157.78, 155.96, 136.54 (2C), 130.41, 125.82, 125.15, 121.94, 120.33, 118.27, 117.00, 103.74 (2C), 98.01, 93.79, 66.31, 59.10, 55.41, 52.51, 27.02. HRMS: calcd for $C_{24}H_{24}NO_5$ $[M+H]^+$ 406.1649, found 406.1604. HPLC purity, 99.15%.

4.4.2. 1-Hydroxy-3-(4-((3-hydroxybenzyl) (methyl)amino)butoxy)-9H-xanthen-9-one (**4b**)

It was prepared from 3-(4-bromobutoxy)-1-hydroxy-9H-xanthen-9-one (**3b**) and 3-((methylamino)methyl)phenol according to the general procedure, then purified on a silica gel chromatography eluted with dichloromethane/methanol (25:1) to obtain the pure product **4b**. 71% yield; yellow solid; m.p. 157–161 °C; ^{1}H NMR (600 MHz, DMSO) δ 12.82 (s, 1H), 9.72 (s, 1H), 8.17 (dd, *J* = 7.8, 1.8 Hz, 1H), 7.92–7.89 (m, 1H), 7.63 (d, *J* = 8.4 Hz, 1H), 7.53–7.50 (m, 1H), 7.26 (t, *J* = 7.8 Hz, 1H), 6.93–6.91 (m, 2H), 6.86 (dd, *J* = 8.4, 1.8 Hz, 1H), 6.66 (d, *J* = 2.4 Hz, 1H), 6.42 (d, *J* = 2.4 Hz, 1H), 4.33 (d, *J* = 12.0 Hz, 1H), 4.17 (t, *J* = 6.0 Hz, 3H), 3.21 (s, 1H), 3.10–3.09 (m, 1H), 2.69 (s, 3H), 1.88–1.77 (m, 4H). ^{13}C NMR (151 MHz, DMSO) δ 180.60, 166.36, 163.07, 157.92, 157.77, 155.93, 136.44, 130.04 (2C), 125.78, 125.07 (2C), 120.31, 118.23 (2C), 103.57 (2C), 97.95, 93.72, 68.64, 48.94, 30.57, 29.47, 26.20, 17.69. HRMS: calcd for $C_{25}H_{26}NO_5$ $[M+H]^+$ 420.1805, found 420.1757. HPLC purity, 98.94%.

4.4.3. 1-Hydroxy-3-((5-((3-hydroxybenzyl) (methyl)amino)pentyl) oxy)-9H-xanthen-9-one (**4c**)

It was prepared from 3-((5-bromopentyl)oxy)-1-hydroxy-9H-xanthen-9-one (**3c**) and 3-((methylamino)methyl)phenol according to the general procedure, then purified on a silica gel chromatography eluted with dichloromethane/methanol (25:1) to obtain the pure product **4c**. 65% yield; yellow solid; m.p. 200–202 °C; ^{1}H NMR (600 MHz, DMSO) δ 12.81 (s, 1H), 9.73 (s, 1H), 8.17 (dd, *J* = 8.4,

1.8 Hz, 1H), 7.91–7.88 (m, 1H), 7.63 (d, J = 8.3 Hz, 1H), 7.52–7.50 (m, 1H), 7.27 (t, J = 7.8 Hz, 1H), 6.93–6.86 (m, 3H), 6.66 (d, J = 2.4 Hz, 1H), 6.42 (d, J = 2.4 Hz, 1H), 4.32 (d, J = 12.0 Hz, 1H), 4.15 (t, J = 6.3 Hz, 3H), 3.13–3.09 (m, 2H), 2.65 (s, 3H), 1.81–1.74 (m, 4H), 1.47–1.42 (m, 2H). ^{13}C NMR (151 MHz, DMSO) δ 180.61, 166.44, 163.09, 158.08, 157.79, 155.94, 136.47, 131.77, 130.44, 125.79, 125.10, 121.98, 120.32, 118.26, 118.23, 116.98, 103.57, 97.94, 93.73, 68.72, 58.94, 55.21, 46.22, 28.23, 23.40, 23.01. HRMS: calcd for $C_{26}H_{28}NO_5$ $[M+H]^+$ 434.1962, found 434.1902. HPLC purity, 99.15%.

4.4.4. 1-Hydroxy-3-((6-((3-hydroxybenzyl) (methyl)amino)hexyl) oxy)-9H-xanthen-9-one (**4d**)

It was prepared from 3-((6-bromohexyl)oxy)-1-hydroxy-9H-xanthen-9-one (**3d**) and 3-((methylamino)methyl)phenol according to the general procedure, then purified on a silica gel chromatography eluted with dichloromethane/methanol (25:1) to obtain the pure product **4d**. 67% yield; yellow solid; m.p. 106–110 °C; ^{1}H NMR (600 MHz, DMSO) δ 12.81 (s, J = 7.8, 1.8 Hz, 1H), 9.72 (s, 1H), 8.16 (dd, J = 7.9, 1.6 Hz, 1H), 7.91–7.88 (m, 1H), 7.62 (d, J = 8.4 Hz, 1H), 7.52–7.49 (m, 1H), 7.27 (t, J = 7.8 Hz, 1H), 6.92–6.86 (m, 3H), 6.65 (d, J = 1.8 Hz, 1H), 6.41 (d, J = 2.4 Hz, 1H), 4.31 (d, J = 11.4 Hz, 1H), 4.14 (t, J = 6.0 Hz, 3H), 3.12–3.09 (m, 1H), 3.00 (s, 1H), 2.67 (s, 3H), 1.79–1.69 (m, 4H), 1.47–1.43 (m, 2H), 1.36–1.34 (m, 2H). ^{13}C NMR (151 MHz, DMSO) δ 180.60, 166.50, 163.09, 158.07, 157.80, 155.94, 136.46, 131.81, 130.44, 125.79, 125.09, 121.95, 120.32, 118.23, 116.96, 103.55 (2C), 97.92, 93.70, 68.94, 58.93, 55.25, 46.21, 28.52, 26.07, 25.38, 23.66. HRMS: calcd for $C_{27}H_{30}NO_5$ $[M+H]^+$ 448.2118, found 448.2050. HPLC purity, 99.62%.

4.4.5. 1-Hydroxy-3-((7-((3-hydroxybenzyl) (methyl)amino)heptyl) oxy)-9H-xanthen-9- one (**4e**)

It was prepared from 3-((7-bromoheptyl)oxy)-1-hydroxy-9H-xanthen-9-one (**3e**) and 3-((methylamino)methyl)phenol according to the general procedure, then purified on a silica gel chromatography eluted with dichloromethane/methanol (25:1) to obtain the pure product **4e**. 68% yield; yellow solid; m.p. 121–124 °C; ^{1}H NMR (600 MHz, DMSO) δ 12.80 (s, 1H), 9.72 (s, 1H), 8.16 (d, J = 7.8 Hz, 1H), 7.89 (t, J = 8.4 Hz, 1H), 7.62 (d, J = 8.4 Hz, 1H), 7.50 (t, J = 7.8 Hz, 1H), 7.26 (t, J = 7.2 Hz, 1H), 6.91–6.85 (m, 3H), 6.65 (s, 1H), 6.40 (s, 1H), 4.29 (s, 1H),4.13 (d, J = 6.0 Hz, 3H), 3.04 (d, J = 54.6 Hz, 2H), 2.66 (s, 3H), 1.42 (d, J = 6.6 Hz, 2H), 1.37–1.22 (m, 8H). ^{13}C NMR (151 MHz, DMSO) δ 180.60, 166.53, 163.08, 158.07, 157.79, 155.93, 136.45, 131.83, 130.43, 125.78, 125.08, 121.92, 120.31, 118.23, 116.93, 103.53 (2C), 97.91, 93.69, 69.04, 58.96, 55.32, 48.94, 28.68, 28.59, 26.34, 25.62, 23.68. HRMS: calcd for $C_{28}H_{32}NO_5$ $[M+H]^+$ 462.2275, found 462.2183. HPLC purity, 98.12%.

4.4.6. 1-Hydroxy-3-((8-((3-hydroxybenzyl) (methyl)amino)octyl) oxy)-9H-xanthen-9-one (**4f**)

It was prepared from 3-((8-bromooctyl)oxy)-1-hydroxy-9H-xanthen-9-one (**3f**) and 3-((methylamino)methyl)phenol according to the general procedure, then purified on a silica gel chromatography eluted with dichloromethane/methanol (25:1) to obtain the pure product **4f**. 65% yield; yellow solid; m.p. 124–127 °C; ^{1}H NMR (600 MHz, DMSO) δ 12.81 (s, 1H), 9.72 (s, 1H), 8.16 (d, J = 6.0 Hz, 1H), 7.89 (t, J = 8.4 Hz, 1H), 7.62 (d, J = 7.8 Hz, 1H), 7.52–7.49 (m, 1H), 7.27 (t, J = 7.8 Hz, 1H), 6.91–6.85 (m, 3H), 6.65 (d, J = 1.8 Hz, 1H), 6.40 (d, J = 1.2 Hz, 1H), 4.29 (s, 1H), 4.13 (t, J = 6.0 Hz, 3H), 3.08 (s, 1H), 2.98 (s, 1H), 2.66 (s, 3H), 1.77–1.67 (m, 4H), 1.43–1.40 (m, 2H), 1.33–1.30 (m, 6H). ^{13}C NMR (151 MHz, DMSO) δ 180.59, 166.54, 163.08, 158.07, 157.79, 155.93, 136.44, 131.81, 130.43, 125.78, 125.07, 121.93, 120.32, 118.23, 116.94, 103.52 (2C), 97.91, 93.69, 69.07 (2C), 58.92, 55.29, 28.88, 28.86, 28.78, 26.35, 25.75, 23.69. HRMS: calcd for $C_{29}H_{34}NO_5$ $[M+H]^+$ 476.2431, found 476.2363. HPLC purity, 98.56%.

4.4.7. 1-Hydroxy-3-(3-((4-hydroxybenzyl) (methyl)amino) propoxy)-9H-xanthen-9-one (**4g**)

It was prepared from 3-(3-bromopropoxy)-1-hydroxy-9H-xanthen-9-one (**3a**) and 4-((methylamino)methyl)phenol according to the general procedure, then purified on a silica gel chromatography eluted with dichloromethane/methanol (25:1) to obtain the pure product **4g**. 61% yield; yellow solid; m.p. 178–180 °C; ^{1}H NMR (600 MHz, DMSO) δ 12.82 (s, 1H), 9.81 (s, 1H), 8.17 (d, J = 8.4 Hz, 1H), 7.92–7.89 (m, 1H), 7.64 (d, J = 8.4 Hz, 1H), 7.52 (d, J = 7.2 Hz, 1H), 7.33 (d, J = 7.8 Hz, 2H), 6.84 (d, J = 9.0 Hz, 2H), 6.66 (s, 1H), 6.41 (s, 1H), 4.32 (s, 1H), 4.22 (d, J = 6.0 Hz, 3H), 3.29 (s, 2H), 2.70 (s, 3H), 2.18 (s, 2H). ^{13}C NMR (151 MHz, DMSO) δ 180.67, 165.95, 163.07, 158.97, 157.77, 155.95, 136.54, 133.21 (2C), 125.81, 125.15 (2C), 120.31 (2C), 118.27, 116.01, 103.74, 98.00, 93.79, 66.27, 58.79, 52.02, 46.23, 23.85. HRMS: calcd for $C_{24}H_{24}NO_5$ $[M+H]^+$ 406.1649, found 406.1608. HPLC purity, 98.68%.

4.4.8. 1-Hydroxy-3-(4-((4-hydroxybenzyl) (methyl)amino)butoxy)-9H-xanthen-9-one (**4h**)

It was prepared from 3-(4-bromobutoxy)-1-hydroxy-9H-xanthen-9-one (**3b**) and 4-((methylamino)methyl)phenol according to the general procedure, then purified on a silica gel chromatography eluted with dichloromethane/methanol (25:1) to obtain the pure product **4h**. 59% yield; yellow solid; m.p. 150–153 °C; ^{1}H NMR (600 MHz, DMSO) δ 12.82 (s, 1H), 9.80 (s, 1H), 8.17 (dd, J = 7.8, 1.2 Hz, 1H), 7.92–7.89 (m, 1H), 7.64 (d, J = 8.4 Hz, 1H), 7.52 (d, J = 7.2 Hz, 1H), 7.32 (d, J = 8.4 Hz, 2H), 6.82 (d, J = 8.4 Hz, 2H), 6.67 (d, J = 2.4 Hz, 1H), 6.43 (d, J = 1.8 Hz, 1H), 4.28 (d, J = 12.0 Hz, 1H), 4.18–4.14 (m, 3H), 3.18 (s, 1H), 3.04 (s, 1H), 2.66 (s, 3H), 1.87–1.77 (m, 4H). ^{13}C NMR (151 MHz, DMSO) δ 180.64, 166.26, 163.09, 158.96, 157.79, 155.95, 136.50, 133.23 (3C), 125.80, 125.13, 120.33, 118.25, 115.99 (2C), 103.63, 97.98, 93.78, 68.39, 58.63, 54.47, 46.21, 25.91, 20.85. HRMS: calcd for $C_{25}H_{26}NO_5$ $[M+H]^+$ 420.1805, found 420.1746. HPLC purity, 95.12%.

4.4.9. 1-Hydroxy-3-((5-((4-hydroxybenzyl) (methyl)amino)pentyl) oxy)-9H-xanthen-9-one (**4i**)

It was prepared from 3-((5-bromopentyl)oxy)-1-hydroxy-9H-xanthen-9-one (**3c**) and 4-((methylamino)methyl)phenol according to the general procedure, then purified on a silica gel chromatography eluted with dichloromethane/methanol (25:1) to obtain the pure product **4i**. 63% yield; yellow solid; m.p. 221–223 °C; ^{1}H NMR (600 MHz, DMSO) δ 12.81 (s, 1H), 9.81 (s, 1H), 8.16 (dd, J = 7.8, 1.8 Hz, 1H), 7.91–7.88 (m, 1H), 7.62 (d, J = 8.4 Hz, 1H), 7.51 (d, J = 7.2 Hz, 1H), 7.32 (d, J = 8.4 Hz, 2H), 6.83 (d, J = 8.4 Hz, 2H), 6.66 (d, J = 2.4 Hz, 1H), 6.41 (d, J = 1.8 Hz, 1H), 4.28 (d, J = 12.6 Hz, 1H), 4.15 (d, J = 6.0 Hz, 2H), 4.11 (d, J = 9.0 Hz, 1H), 3.10 (d, J = 4.8 Hz, 1H), 2.98 (s, 1H), 2.65 (s, 3H), 1.80–1.73 (m, 4H), 1.46–1.42 (m, 2H). ^{13}C NMR (151 MHz, DMSO) δ 180.61, 166.44, 163.08, 158.95, 157.79, 155.93, 136.47, 133.20 (3C), 125.79, 125.09, 120.31, 118.23, 116.01 (2C), 103.56, 97.93, 93.72, 68.73, 58.62, 54.72, 38.97, 28.23, 23.45, 23.03. HRMS: calcd for $C_{26}H_{28}NO_5$ $[M+H]^+$ 434.1962, found 434.1897. HPLC purity, 98.18%.

4.4.10. 1-Hydroxy-3-((6-((4-hydroxybenzyl) (methyl)amino)hexyl) oxy)-9H-xanthen-9-one (**4j**)

It was prepared from 3-((6-bromohexyl)oxy)-1-hydroxy-9H-xanthen-9-one (**3d**) and 4-((methylamino)methyl)phenol according to the general procedure, then purified on a silica gel chromatography eluted with dichloromethane/methanol (25:1) to obtain the pure product **4j**. 70% yield; yellow solid; m.p. 113–116 °C; ^{1}H NMR (600 MHz, DMSO) δ 12.81 (s, 1H), 9.80 (s, 1H), 8.17 (dd, J = 7.8, 1.8 Hz, 1H), 7.91–7.88 (m, 1H), 7.63 (d, J = 8.4 Hz, 1H), 7.51 (d, J = 7.8 Hz, 1H), 7.31 (d, J = 8.4 Hz, 2H), 6.83 (d, J = 8.4 Hz, 2H), 6.66 (d, J = 2.4 Hz, 1H), 6.41 (d, J = 1.8 Hz, 1H), 4.27 (d, J = 12.6 Hz, 1H),

4.15–4.10 (m, 3H), 3.09 (s, 1H), 2.95 (s, 1H), 2.65 (s, 3H), 1.78–1.68 (m, 4H), 1.47–1.42 (m, 2H), 1.37–1.33 (m, 2H). ^{13}C NMR (151 MHz, DMSO) δ 180.61, 166.51, 163.09, 158.94, 157.80, 155.94, 136.47, 133.18 (3C), 125.79, 125.09, 120.32, 118.24, 116.01 (2C), 103.55, 97.93, 93.71, 68.94, 58.62, 54.79, 46.21, 28.52, 26.09, 25.37, 23.71. HRMS: calcd for $C_{27}H_{30}NO_5$ $[M+H]^+$ 448.2118, found 448.2060. HPLC purity, 99.44%.

4.4.11. 1-Hydroxy-3-((7-((4-hydroxybenzyl) (methyl)amino)heptyl) oxy)-9H-xanthen-9-one (**4k**)

It was prepared from 3-((7-bromoheptyl)oxy)-1-hydroxy-9H-xanthen-9-one (**3e**) and 4-((methylamino)methyl)phenol according to the general procedure, then purified on a silica gel chromatography eluted with dichloromethane/methanol (25:1) to obtain the pure product **4k**. 75% yield; yellow solid; m.p. 128–130 °C; ^{1}H NMR (600 MHz, DMSO) δ 12.81 (s, 1H), 9.79 (s, 1H), 8.17 (dd, *J* = 7.8, 1.8 Hz, 1H), 7.91–7.89 (m, 1H), 7.63 (d, *J* = 8.4 Hz, 1H), 7.52–7.50 (m, 1H), 7.31 (d, *J* = 8.4 Hz, 2H), 6.83 (d, *J* = 8.4 Hz, 2H), 6.66 (d, *J* = 1.8 Hz, 1H), 6.41 (d, *J* = 1.8 Hz, 1H), 4.26 (d, *J* = 13.2 Hz, 1H), 4.14 (t, *J* = 6.6 Hz, 3H), 3.00–2.95 (m, 2H), 2.64 (s, 3H), 1.77–1.70 (m, 4H), 1.44–1.41 (m, 2H), 1.37–1.35 (m, 2H), 1.23 (t, *J* = 4.8 Hz, 2H). ^{13}C NMR (151 MHz, DMSO) δ 180.62, 166.55, 163.09, 158.94, 157.82, 155.94, 136.48, 133.19 (3C), 125.10, 120.40, 120.33, 118.25, 116.00 (2C), 103.55, 97.94, 93.72, 69.06, 58.59, 54.83, 53.15, 28.68, 28.57, 26.33, 25.61, 25.51. HRMS: calcd for $C_{28}H_{31}NO_5$ $[M+H]^+$ 462.2275, found 462.2193. HPLC purity, 96.15%.

4.4.12. 1-Hydroxy-3-((8-((4-hydroxybenzyl) (methyl)amino)octyl) oxy)-9H-xanthen-9-one (**4l**)

It was prepared from 3-((8-bromooctyl)oxy)-1-hydroxy-9H-xanthen-9-one (**3f**) and 4-((methylamino)methyl)phenol according to the general procedure, then purified on a silica gel chromatography eluted with dichloromethane/methanol (25:1) to obtain the pure product **4l**. 81% yield; yellow solid; m.p. 125–127 °C; ^{1}H NMR (600 MHz, DMSO) δ 12.81 (s, 1H), 9.80 (s, 1H), 8.16 (dd, *J* = 7.8, 1.8 Hz, 1H), 7.91–7.88 (m, 1H), 7.62 (d, *J* = 8.4 Hz, 1H), 7.51 (d, *J* = 7.8 Hz, 1H), 7.30 (d, *J* = 8.4 Hz, 2H), 6.83 (d, *J* = 8.4 Hz, 2H), 6.65 (d, *J* = 1.8 Hz, 1H), 6.40 (d, *J* = 2.4 Hz, 1H), 4.25 (d, *J* = 12.6 Hz, 1H), 4.14–4.10 (m, 3H), 3.06 (s, 1H), 2.94 (s, 1H), 2.64 (s, 3H), 1.77–1.72 (m, 2H), 1.68–1.64 (m, 2H), 1.43–1.39 (m, 2H), 1.35–1.30 (m, 6H). ^{13}C NMR (151 MHz, DMSO) δ 180.62, 166.56, 163.10, 158.95, 157.81, 155.95, 136.47, 133.18 (3C), 125.79, 125.09, 120.33, 118.25, 116.01 (2C), 103.54, 97.93, 93.71, 69.08, 58.62, 54.83, 46.22, 28.88, 28.85, 28.78, 26.36, 25.74, 23.74. HRMS: calcd for $C_{29}H_{34}NO_5$ $[M+H]^+$ 476.2431, found 476.2357. HPLC purity, 97.20%.

4.4.13. 1-Hydroxy-3-((6-((4-methoxybenzyl) (methyl)amino)hexyl) oxy)-9H-xanthen-9-one (**4m**)

It was prepared from 3-((6-bromohexyl)oxy)-1-hydroxy-9H-xanthen-9-one (**3d**) and 1-(4-methoxyphenyl)-N-methylmethanamine according to the general procedure, then purified on a silica gel chromatography eluted with dichloromethane/methanol (25:1) to obtain the pure product **4m**. 69% yield; yellow solid; m.p. 70–72 °C; ^{1}H NMR (600 MHz, $CDCl_3$) δ 12.88 (s, 1H), 8.27 (dd, *J* = 8.4, 1.8 Hz, 1H), 7.74–7.71 (m, 1H), 7.44 (d, *J* = 8.4 Hz, 1H), 7.41–7.38 (m, 1H), 7.25 (d, *J* = 8.4 Hz, 2H), 6.88 (d, *J* = 9.0 Hz, 2H), 6.44 (d, *J* = 2.4 Hz, 1H), 6.36 (d, *J* = 2.4 Hz, 1H), 4.06 (t, *J* = 6.0 Hz, 2H), 3.82 (s, 3H), 3.49 (s, 2H), 2.42 (t, *J* = 7.2 Hz, 2H), 2.23 (s, 3H), 1.86–1.82 (m, 2H), 1.62–1.57 (m, 2H), 1.52–1.47 (m, 2H), 1.43–1.40 (m, 2H). ^{13}C NMR (151 MHz, $CDCl_3$) δ 180.78, 166.34, 163.52, 158.73, 157.74, 156.04, 134.96, 130.38 (3C), 125.87, 123.98, 120.66, 117.58, 113.61, 103.83 (2C), 97.46, 93.24, 68.62, 61.51, 56.96, 55.25, 41.93, 28.91, 27.09, 27.05, 25.86. HRMS: calcd for $C_{28}H_{32}NO_5$ $[M+H]^+$ 462.2275, found 462.2187. HPLC purity, 98.81%.

4.4.14. 3-((6-(ethyl(4-hydroxybenzyl)amino)hexyl)oxy)-1-hydroxy-9H-xanthen-9-one (**4n**)

It was prepared from 3-((6-bromohexyl)oxy)-1-hydroxy-9H-xanthen-9-one (**3d**) and 4-((ethylamino)methyl)phenol according to the general procedure, then purified on a silica gel chromatography eluted with dichloromethane/methanol (25:1) to obtain the pure product **4n**. 74% yield; yellow solid; m.p. 74–75 °C; ^{1}H NMR (600 MHz, DMSO) δ 12.74 (s, 1H), 9.26 (s, 1H), 8.15 (d, *J* = 7.8 Hz, 1H), 7.88 (t, *J* = 7.8 Hz, 1H), 7.62 (d, *J* = 8.4 Hz, 1H), 7.50 (t, *J* = 7.2 Hz, 1H), 7.07 (d, *J* = 8.4 Hz, 2H), 6.68 (d, *J* = 8.4 Hz, 2H), 6.63 (s, 1H), 6.39 (s, 1H), 4.10 (t, *J* = 6.6 Hz, 2H), 2.42–2.39 (m, 2H), 2.34 (t, *J* = 7.2 Hz, 2H), 1.71 (t, *J* = 7.2 Hz, 2H), 1.42 (t, *J* = 7.2 Hz, 2H), 1.38 (t, *J* = 7.8 Hz, 2H), 1.30 (t, *J* = 6.6 Hz, 4H), 0.95 (t, *J* = 7.2 Hz, 3H). ^{13}C NMR (151 MHz, DMSO) δ 180.58, 166.56, 163.08, 157.79, 156.52, 155.93, 136.40, 130.13 (3C), 125.76, 125.03, 120.32, 118.23, 115.25, 103.51 (2C), 97.93, 93.67, 69.05, 57.28, 52.52, 46.84, 28.83, 26.97, 25.69, 22.56, 11.98. HRMS: calcd for $C_{28}H_{32}NO_5$ $[M+H]^+$ 462.2275, found 462.2198. HPLC purity, 97.95%.

4.5. General procedure for the synthesis of carbamates (**5a-f**)

A mixture of the selected 1-hydroxyl-3-aminoalkoxyxanthen derivative (0.22 mmol), the selected isocyanate (1.1 mmol) and triethylamine (0.43 mmol) in dry DMF, under nitrogen atmosphere, was stirred at room temperature for 36–48 h. Upon completion of the reaction, the mixture was pulled into water stirring for minutes and extracted with ethyl acetate (10 ml × 3). The ethyl acetate layer was collected, dried over anhydrous sodium sulfate, filtered and concentrated under reduced pressure to give the compounds **5a-f**.

4.5.1. 4-(((6-((1-hydroxy-9-oxo-9H-xanthen-3-yl)oxy)hexyl) (methyl)amino)methyl) phenyl ethylcarbamate (**5a**)

Using the previous procedure and starting from **4j** and isocyanatoethane, **5a** was obtained. 48% yield; yellow solid; m.p. 103–106 °C; ^{1}H NMR (600 MHz, $CDCl_3$) δ 12.88 (s, 1H), 8.26 (dd, *J* = 7.8, 1.8 Hz, 1H), 7.74–7.71 (m, 1H), 7.45 (d, *J* = 8.4 Hz, 1H), 7.40–7.38 (m, 1H), 7.30 (d, *J* = 8.4 Hz, 2H), 7.07 (d, *J* = 8.4 Hz, 2H), 6.44 (d, *J* = 1.8 Hz, 1H), 6.36 (d, *J* = 2.4 Hz, 1H), 5.19 (s, 1H), 4.04 (t, *J* = 6.6 Hz, 2H), 3.47 (s, 2H), 3.34–3.29 (m, 2H), 2.37 (t, *J* = 7.8 Hz, 2H), 2.21 (s, 3H), 1.83–1.81 (m, 2H), 1.58–1.53 (m, 2H), 1.47–1.45 (m, 2H), 1.42–1.39 (m, 2H), 1.24–1.21 (m, 3H). ^{13}C NMR (151 MHz, $CDCl_3$) δ 180.82, 166.41, 163.46, 158.46, 157.75, 156.06, 149.93, 135.00, 129.82 (3C), 125.84, 123.99, 121.30, 120.63, 117.60, 103.81 (2C), 97.50, 93.28, 68.68, 61.78, 57.00, 42.26, 36.12, 28.91, 27.19, 26.98, 25.79, 15.11. HRMS: calcd for $C_{30}H_{35}N_2O_6$ $[M+H]^+$ 519.2489, found 519.2392. HPLC purity, 98.81%.

4.5.2. 4-(((6-((1-hydroxy-9-oxo-9H-xanthen-3-yl)oxy)hexyl) (methyl)amino)methyl) phenyl (2-chloroethyl)carbamate (**5b**)

Using the previous procedure and starting from **4j** and 1-chloro-2-isocyanatoethane, **5b** was obtained. 45% yield; yellow solid; m.p. 121–124 °C; ^{1}H NMR (600 MHz, $CDCl_3$) δ 12.88 (br s, 1H), 8.27 (dd, *J* = 7.8, 1.2 Hz, 1H), 7.74–7.71 (m, 1H), 7.45 (d, *J* = 8.4 Hz, 1H), 7.41–7.36 (m, 3H), 7.12 (d, *J* = 8.4 Hz, 2H), 6.44 (d, *J* = 2.4 Hz, 1H), 6.36 (d, *J* = 1.8 Hz, 1H), 5.09 (s, 1H), 4.05 (d, *J* = 6.0 Hz, 2H), δ 3.70 (t, *J* = 5.4 Hz, 2H), 3.65–3.62 (m, 3H), 3.56 (t, *J* = 6.0 Hz, 1H),2.47 (t, *J* = 7.2 Hz, 2H), 2.29 (s, 3H), 1.85–1.80 (m, 2H), 1.65–1.60 (m, 2H), 1.50–1.45 (m, 2H), 1.43–1.39 (m, 2H). ^{13}C NMR (151 MHz, $CDCl_3$) δ 180.80, 166.35, 163.47, 157.74, 157.37, 156.05, 150.11, 134.99, 130.27 (3C), 125.86, 123.99, 121.44, 120.64, 117.60, 103.83 (2C), 97.49, 93.27, 68.60, 61.36, 56.68, 43.89, 42.99, 41.84, 28.87, 26.89, 26.66, 25.74. HRMS: calcd for $C_{30}H_{34}ClN_2O_6$ $[M+H]^+$ 553.2099, found 553.1986. HPLC purity, 97.28%.

*4.5.3. 4-(((6-((1-hydroxy-9-oxo-9H-xanthen-3-yl)oxy)hexyl) (methyl)amino)methyl) phenyl cyclohexylcarbamate (**5c**)*

Using the previous procedure and starting from **4j** and isocyanatocyclohexane, **5c** was obtained. 44% yield; yellow solid; m.p. 126–128 °C; ^{1}H NMR (600 MHz, $CDCl_3$) δ 12.89 (s, 1H), 8.27 (dd, J = 7.8, 1.2 Hz, 1H), 7.74–7.71 (m, 1H), 7.45 (d, J = 8.4 Hz, 1H), 7.41–7.38 (m, 1H), 7.30 (d, J = 8.4 Hz, 2H), 7.09 (d, J = 8.4 Hz, 2H), 6.44 (d, J = 2.4 Hz, 1H), 6.37 (d, J = 1.8 Hz, 1H), 4.97 (d, J = 7.8 Hz, 1H), 4.05 (t, J = 6.0 Hz, 2H), 3.59–3.54 (m, 1H), 3.49 (s, 2H), 2.38 (t, J = 7.2 Hz, 2H), 2.22 (s, 3H), 2.02 (d, J = 9.0 Hz, 2H), 1.85–1.73 (m, 8H), 1.65–1.53 (m, 4H), 1.48–1.46 (m, 2H), 1.42–1.40 (m, 2H). ^{13}C NMR (151 MHz, $CDCl_3$) δ 180.79, 166.39, 163.49, 157.73, 156.05, 153.77, 150.01, 134.96, 129.83 (3C), 125.86, 123.97, 121.30, 120.65, 117.59, 103.82 (2C), 97.50, 93.27, 68.67, 61.75, 56.96, 50.11, 42.23, 33.26 (2C), 28.92, 27.16, 27.00, 25.81, 25.46, 24.76 (2C). HRMS: calcd for $C_{34}H_{40}N_2O_6$ $[M+H]^+$ 573.2959, found 573.2837. HPLC purity, 95.57%.

*4.5.4. 4-((ethyl(6-((1-hydroxy-9-oxo-9H-xanthen-3-yl)oxy)hexyl) amino)methyl) phenyl ethylcarbamate (**5d**)*

Using the previous procedure and starting from **4n** and isocyanatoethane, **5d** was obtained. 45% yield; yellow solid; m.p. 85–88 °C; ^{1}H NMR (600 MHz, $CDCl_3$) δ 12.89 (s, 1H), 8.27 (dd, J = 7.8, 1.2 Hz, 1H), 7.74–7.72 (m, 1H), 7.45 (d, J = 7.8 Hz, 1H), 7.39 (d, J = 7.8 Hz, 1H), 7.32 (d, J = 8.4 Hz, 2H), 7.07 (d, J = 7.8 Hz, 2H), 6.44 (d, J = 2.4 Hz, 1H), 6.37 (d, J = 2.4 Hz, 1H), 5.08 (s, 1H), 4.03 (d, J = 6.6 Hz, 2H), 3.55 (s, 2H), 3.33–3.31 (m, 2H), 2.55–2.51 (m, 2H), 2.44 (t, J = 7.2 Hz, 2H), 1.81 (d, J = 6.6 Hz, 2H), 1.51 (t, J = 7.8 Hz, 2H), 1.45–1.42 (m, 2H), 1.39–1.37 (m, 2H), 1.23 (t, J = 7.2 Hz, 3H), 1.05 (d, J = 7.2 Hz, 3H). ^{13}C NMR (151 MHz, $CDCl_3$) δ 180.80, 166.42, 163.48, 157.73, 156.06, 154.62, 149.78, 134.97 (2C), 129.58 (2C), 125.86, 123.97, 121.22 (2C), 120.65, 117.59, 103.81, 97.50, 93.29, 68.69, 57.50, 52.75, 47.27, 36.12, 28.93, 26.99 (2C), 25.75, 15.14, 11.72. HRMS: calcd for $C_{31}H_{37}N_2O_6$ $[M+H]^+$ 533.2646, found 533.2527. HPLC purity, 97.43%.

*4.5.5. 4-((ethyl(6-((1-hydroxy-9-oxo-9H-xanthen-3-yl)oxy)hexyl) amino)methyl) phenyl (2-chloroethyl)carbamate (**5e**)*

Using the previous procedure and starting from **4n** and 1-chloro-2-isocyanatoethane, **5e** was obtained. 45% yield; yellow solid; m.p. 66–68 °C; ^{1}H NMR (600 MHz, $CDCl_3$) δ 12.89 (br s, 1H), 8.26 (dd, J = 7.8, 1.8 Hz, 1H), 7.74–7.71 (m, 1H), 7.45 (d, J = 8.4 Hz, 1H), 7.40–7.38 (m, 3H), 7.10 (d, J = 8.4 Hz, 2H), 6.44 (d, J = 2.4 Hz, 1H), 6.36 (d, J = 2.4 Hz, 1H), 5.15 (s, 1H),4.03 (d, J = 6.0 Hz, 2H), 3.70 (t, J = 5.4 Hz, 2H), 3.64–3.62 (m, 3H), 3.56 (t, J = 6.0 Hz, 1H), 2.61 (s, 2H), 2.51 (s, 2H), 1.82–1.80 (m, 2H), 1.57 (s, 2H), 1.47–1.42 (m, 2H), 1.40–1.37 (m, 2H), 1.11 (s, 3H). ^{13}C NMR (151 MHz, $CDCl_3$) δ 180.82, 166.38, 163.48, 157.74, 157.45, 156.06, 154.63, 135.00 (2C), 130.01 (2C), 125.87, 124.00, 121.35, 120.65, 117.60 (2C), 103.83, 97.50, 93.29, 68.63, 64.33, 57.24, 52.51, 43.00, 42.14, 28.89, 26.91 (2C), 25.70, 11.30. HRMS: calcd for $C_{31}H_{36}ClN_2O_6$ $[M+H]^+$ 567.2256, found 567.2134. HPLC purity, 96.68%.

*4.5.6. 4-((ethyl(6-((1-hydroxy-9-oxo-9H-xanthen-3-yl)oxy)hexyl) amino)methyl) phenyl cyclohexylcarbamate (**5f**)*

Using the previous procedure and starting from **4n** and isocyanatocyclohexane, **5f** was obtained. 43% yield; yellow solid; m.p. 80–83 °C; ^{1}H NMR (600 MHz, $CDCl_3$) δ 12.89 (s, 1H), 8.27 (dd, J = 8.4, 1.8 Hz, 1H), 7.74–7.72 (m, 1H), 7.45 (d, J = 8.4 Hz, 1H), 7.41–7.38 (m, 1H), 7.33 (t, J = 7.8 Hz, 2H), 7.07 (d, J = 7.8 Hz, 2H), 6.44 (d, J = 2.4 Hz, 1H), 6.37 (d, J = 2.4 Hz, 1H), 4.98 (d, J = 7.8 Hz, 1H), 4.03 (t, J = 6.6 Hz, 2H), 3.53 (s, 1H), 3.50 (s, 2H), 2.55–2.51 (m, 2H), 2.45–2.43 (m, 2H), 1.82–1.79 (m, 2H), 1.65–1.60 (m, 4H), 1.54–1.49 (m, 2H), 1.38–1.35 (m, 6H), 1.23 (d, J = 10.2 Hz, 3H), 1.07–1.04 (m, 4H). ^{13}C NMR (151 MHz, $CDCl_3$) δ 180.80, 166.41, 163.49, 157.73, 156.76, 156.06, 149.82, 134.96, 129.99, 129.57, 129.41, 125.86, 123.97, 121.21, 120.66, 117.60, 115.08, 103.81, 97.50, 93.29, 68.69, 57.49, 52.75, 50.10, 47.25, 33.96 (2C), 28.93, 27.00 (2C), 26.85, 25.62, 24.95 (2C), 11.84. HRMS: calcd for $C_{35}H_{43}N_2O_6$ $[M+H]^+$ 587.3115, found 587.2982. HPLC purity, 99.56%.

5. Biological evaluation

5.1. Inhibitory activities of AChE and BuChE

The inhibition activities of target compounds **4a-n** and **5a-f** against ChEs were determined according to Ellman's method. Acetylcholinesterase (AChE) from electric eel (eeAChE), butylcholinesterase (BuChE) from equine serum (eqBuChE), acetylthiocholine iodide (ATCI), S-butylthiocholine iodide (BTCI) and 5,5-dithiobis-(2-nitrobenzoicacid) (DTNB) were purchased from Sigma-Aldrich (St. Louis, MO, USA). For AChE inhibition assay, the target compound was dissolved in DMSO firstly and then diluted to different concentrations with Tris-HCl buffer solution (50 mM, pH = 8.0, 0.1 M NaCl, 0.02 M $MgCl_2 \cdot H_2O$) (DMSO < 0.01%). The experimental protocol was performed on 96-well plate. For each test well, 160 μL of DTNB (1.5 mM), 50 μL of AChE (0.22 U/mL eeAChE) and 10 μL of corresponding concentration of tested compound were added, and then the mixture was incubated at 37 °C for 5 min. After that, 30 μL of ATCI (15 mM) as substrate was quickly added and the absorbance was determined with a wavelength of 405 nm by a UV plate reader at different time intervals (0, 60, 120, and 180 s). For BuChE inhibition assay, the procedure was similar with the method described above. The inhibition activity of tested compound was reported with IC_{50} value that was calculated as concentration of the compound that produced 50% enzyme activity inhibition. The results were expressed as mean ± SD of three independent experiments. Data analysis was performed using Graph Pad Prism 4.03 software (San Diego, CA, USA).

5.2. Free radical scavenging activity on DPPH

The DPPH (1,1-diphenyl-2-picrylhydrazyl radical) assay measures the hydrogen donation ability of the antioxidant to convert the stable DPPH free radical into 1,1-diphenyl-2-(2,4,6-trinitrophenyl)-hydrazine. This can be evaluated by measuring the percent decrease in absorbance of the solution at 517 nm, which is accompanied by a change of color from deep-violet to light-yellow, after the radical reaction with products to be tested. DPPH was dissolved in MeOH to make 10 mM stock solution, which was diluted to 0.1 mM as the test sample. The target compound was dissolved in DMSO to make 10 mM stock solution, which was diluted to five concentrations as test samples. Trolox was used as a standard. The experimental protocol was performed on 96-well plate. For each test well, 100 μL of tested compound, 100 μL of DPPH was added, then was shook and left to incubate at room temperature in the dark for 30 min. Afterwards, the absorbance was determined with a microplate reader, three determinations in parallel, at 517 nm. The percentages of DPPH free radicals were calculated using Equation:

$$\text{DPPH} \cdot \text{free} \cdot \text{radicals} \cdot (\%) \cdot = \cdot [A_0 \cdot - \cdot (A_1 \cdot - \cdot A_2)]/A_0 \cdot \times \cdot 100\%$$

where A_0 is the absorbance of the DPPH radical methanol solution, A_1 is the absorbance of the sample (DPPH + compounds), A_2 is the absorbance of the sample (compounds) alone.

5.3. ABTS radical cation scavenging activity assay

The ABTS radical scavenging capacities of target compounds were measured using a Total Antioxidant Capacity Assay Kit according to the manufacture's instructions. The ABTS radical cation ($ABTS^{+}$) was produced by reacting an aqueous solution of ABTS and oxidant in a ratio of 1:1 (v/v) respectively. The ABTS working solutions were kept to react completely in the dark for 12–16 h, then diluted to an absorbance of 1.4 ± 0.1 at 405 nm with ethanol. To test free radical scavenging effects, compounds and trolox were adjusted with ethanol solution to final concentrations of 0–100 μM. Serial dilutions of the test sample (10 μL) were combined with the ABTS working solution (200 μL) in a 96-wellmicrotitre plate. After 2–6 min in the dark, the absorbance was measured at 405 nm in a microplate reader. Trolox was used as a standard compound.

5.4. Oxygen radical absorbance capacity (ORAC-FL) assay

The antioxidant potency was determined by the oxygen radical absorbance capacity-fluorescein (ORAC-FL) assay with slight modification [40]. 2,2′-Azobis(2-methylpropionamidine) dihydrochloride (AAPH) was purchased from Sigma-Aldrich Chemical Co., Fluorescein (FL) and 6-hydroxy-2,5,7,8-tetramethylchromane-2-carboxylic acid (Trolox) were purchased from TCI (Shanghai) Development. All the assays were carried out in 10 mM phosphate buffer (pH = 7.4), and the final reaction mixture was 200 μL. The tested compound (20 μL) and FL (120 μL, 150 nM final concentration) were placed in the wells of a black 96-well plate and the mixture was pre-incubated for 5 min at 37 °C. Then AAPH solution (60 μL, 12 mM final concentration) was added rapidly using an autosampler and the fluorescence was recorded every 5 min for 90 min with excitation at 485 nm and emission at 538 nm. Trolox was used as standard (0.3125–5 μM, final concentration). A blank (FL + AAPH) using phosphate buffer instead of antioxidant and trolox calibration were carried out in each assay. The samples were measured at different concentration. Antioxidant curves (fluorescence *versus* time) were normalized to the curve of the blank in the same assay (Figure S1), and the area under the fluorescence decay curve (AUC) was calculated using following equation:

$$AUC\cdot = \cdot 5\cdot \times \cdot(f_0\cdot + \cdot f_1\cdot + \cdot ...\cdot + \cdot f_{n-1}\cdot + \cdot f_n)\cdot - \cdot 2.5\cdot \times \cdot(f_0\cdot + \cdot f_n)$$

where f_0 is the initial fluorescence reading at 0 min and f_n is the fluorescence reading at time n.

The net AUC of a sample was obtained by subtracting the AUC of the blank. ORAC-FL values were expressed as Trolox equivalents by using the standard curve calculated for each sample, where the ORAC-FL value of Trolox was taken as 1, indicating the antioxidant potency of the tested compounds.

5.5. PAMPA-BBB penetration assay

The ability of the test compound penetrating into the brain was conducted by a parallel artificial membrane permeation assay (PAMPA) for the blood-brain barrier (BBB) based on previous work of Di et al. Porcine brain lipid (PBL) and dodecane were purchased from Avanti Polar Lipids and Sigma-Aldrich respectively. The donor 96-well filter microplate with a PVDF membrane (pore size 0.45 μM) and acceptor indented 96-well microplate were purchased from Millipore. The 96-well UV plate (COSTAR) was from Corning Incorporated. The acceptor 96-well microplate was filled with 300 μL of PBS/EtOH (7: 3), and the filter membrane was impregnated with 4 μL of PBL in dodecane (20 mg/mL). Compounds were dissolved in DMSO at 5 mg/mL and diluted 50-fold in PBS/EtOH (7:3) to achieve a concentration of 100 μg/mL, 200 μL of which was added to the donor wells. The acceptor filter plate was carefully placed on the donor plate to form a sandwich, which was left undisturbed for 18 h at 25 °C. After incubation, the donor plate was carefully removed and the concentration of compound in the acceptor wells was determined using a UV plate reader (SpectraMax Plus 384, Molecular Devices, Sunnyvale, CA, USA). Every sample was analyzed at five wavelengths, in four wells, in at least three independent runs, and the results are given as the mean ± standard deviation. In each experiment, 9 quality control standards of known BBB permeability were included to validate the analysis set. P_e was calculated by the following expression: $P_e = \{-V_dV_a/[(V_d + V_a)At]\}\ln(1\text{-drug}_{acceptor}/\text{drug}_{equilibrium})$, where V_d is the volume of donor well, V_a is volume in acceptor well, A is the filter area, t is the permeation time, drug acceptor is the absorbance obtained in the acceptor well and drug equilibrium is the theoretical equilibrium absorbance. A good linear correlation was obtained by plotting the experimental data against the bibliographic values: P_e (exp.) = 0.6703 P_e (bibl.) - 0.6571 ($R^2 = 0.9623$).

5.6. Kinetic studies of enzyme inhibition

Compound **4j** was selected for kinetic studies of AChE and BuChE inhibition and performed similar to enzyme inhibition assay. The experiment was performed at four varied concentrations of inhibitor **4j** (0, 0.5, 1, 2 μM for AChE and BuChE), and evaluated against all the six concentrations of substrates (0.05, 0.075, 0.1, 0.15, 0.2, 0.5 mM for ATCI and BTCI). To obtain estimates of the inhibition type, reciprocal plots of 1/V versus 1/[S] were constructed by using reported method with minor modifications. The Dixon plots were generated, and respective K_i values were determined. The assay was conducted in triplicate.

5.7. Molecular docking

The crystal structures of the *hu*AChE, *ee*AChE and *hu*BuChE enzymes were retrieved from the Protein Data Bank (PDB), under the accession codes 4EY7, 2CKM and 1P0I, respectively. Molecular modeling simulation were carried out using the Chemical Computing Group's Molecular Operating Environment (MOE) software (Montreal, Canada, version 2015.10). The protein was energy minimized and 3D protonated using the structure preparation module of MOE. Ligand file for the molecular docking studies were prepared in MOE and were followed by energy optimization at a standard MMFF94 force field level, with a 0.01 kcal/mol energy gradient convergence criterion. Then, the optimized geometry of ligand was saved in a molecular database file and docked into the active site of the protein using the MOE-Dock program. All poses generated with docking were analyzed and the best-scored pose with the lowest binding energy for each compound was selected for further investigation of interactions with the corresponding enzyme.

5.8. Metal-chelating study

The chelating studies were performed with a fluorescence spectrophotometer and an UV–vis spectrophotometer. Stock solutions (1 mM) of the test compound **4j** was prepared by dissolving the sample in DMSO and diluting with a mixture of methanol-water (1/1) to the final concentration of 1 mM. Stock solutions (10 mM) of the cations salts (NaCl, $MgCl_2$, $FeCl_2$, $ZnCl_2$, $CaCl_2$, $AlCl_3$ and $CuCl_2$) were prepared in deionized water. The absorption spectra of ligand (**4j**, 50 μM, final concentration) alone or in the presence of cations salts (50 μM, final concentration) for 30 min

were recorded at room temperature. For the stoichiometry of the **4j**-Cu^{2+} and **4j**-Al^{3+} complexes, a fixed amount of **4j** (50 μM) was mixed with ascending amounts of $CuCl_2$ and $AlCl_3$ respectively. The UV−vis spectra were examined to investigate the ratio of ligand/metals in the complexes.

5.9. Cell culture and toxicity

All cells were obtained from the Cell Bank of the Chinese Academy of Sciences (Shanghai, China). All cells were maintained in high-glucose DMEM supplemented with 10% fetal bovine serum, 100 U/mL penicillin, and 100 U/mL streptomycin in a humidified atmosphere of 5% CO_2 at 37 °C. Cells were subcultured in 96-well plates at a seeding density of 10,000 cells per well and allowed to adhere and grow. When cells reached the required confluence, they were placed into serum-free medium and treated with compounds. After 24 h, the survival of cells was determined by CCK-8 assay according to the manufacture's instructions. Results are expressed as the mean ± SD of three independent experiments.

5.10. Acute toxicity test

A total of 40 KM mice (KunMing mice, 22 days, 18−22 g) purchased from Hunan SJA Laboratory Animal Co., Ltd (eligibility certification No. SCXK [xiang] 2016−0002). Mice were maintained with a 12 h light/dark cycle at 20−22 °C and 60−70% relative humidity. Sterile food and water were provided according to institutional guidelines. Prior to each experiment, mice were fasted overnight and allowed free access to water. Compound **4j** was suspended in 0.5% carboxymethyl cellulose sodium (CMC-Na) salt solution (625, 1250, and 2500 mg/kg) and delivered to tested animals by oral administration. After administration of the compounds, the mice were observed continuously for the first 4 h for any abnormal behavior and mortality changes, intermittently for the next 24 h, and occasionally thereafter for 14 days for the onset of any delayed effects. All animals were sacrificed on the 14th day after drug administration and were macroscopically examined for possible damage to the heart, liver, lung, kidney and brain.

5.11. Step-down test

Kunming mice (male, 18−22g) were purchased from Hunan SJA Laboratory Animal Co., Ltd (eligibility certification No. SCXK [xiang] 2016−0002). The animals were housed in random groups of six per cage, with food and water available. Mice were kept at a temperature of 24 ± 2 °C and a relative humidity of 50−60%, and under a 12-h light-dark cycle. Scopolamine (3 mg/kg, i.p.) from Suicheng Pharmaceutical Co. Ltd. (Zhengzhou, China) was delivered to the mice. Donepezil hydrochloride from the Energy Chemical Co., Ltd (Shanghai, China) was suspended in 0.5% CMC-Na salt solution and delivered to tested animals by oral administration. The mice underwent two separate trials: a training trial and a test trial 24 h later. 24 h after the training trial, the mice were placed on the platform again. The latency to step down on the grid for the first time and the number of shocks received within 5 min were measured as the learning and memory performance.

Declaration of competing interest

The authors declare no conflict of interest.

Acknowledgement

This work was supported by National Natural Science Foundation of China [No. 81760622, 21807052]; Support Program for Outstanding Youth Talents in Jiangxi province [Grant No. 20192BCB23018]; the Program of Natural Science Foundation of Jiangxi province of China [Grant No. 20192ACBL21034, 20202BAB216042]; the 1050 Youth Talent Project of Jiangxi University of Traditional Chinese Medicine [Grant No. 1141900616]; the Open Project Program of Guangxi Key Laboratory of Brain and Cognitive Neuroscience, Guilin Medical University [Grant No. GKLBCN-20200108-07]; Nanchang Double-Hundred Talents Project [Grant No.20200729]; Foundation of Jiangxi Educational Committee [Grant No. GJJ190673].

Appendix A. Supplementary data

Supplementary data to this article can be found online at https://doi.org/10.1016/j.ejmech.2021.113154.

References

[1] M. Prince, A. Wimo, M. Guerchet, G.C. Ail, Y.T. Wu, P.M. World, Alzheimer Report 2015, the Global Impact of Dementia:An Analysis of Prevalence, Incidence, Cost and Trends, Alzheimer's Disease International, London, 2015, pp. 1−88.
[2] M. Wortmann, P4-151: World Alzheimer report 2014: dementia and risk reduction, Alzheimer's Dementia 11 (2015), P837-P837.
[3] C.K. Glass, K. Saijo, B. Winner, M.C. Marchetto, F.H. Gage, Mechanisms underlying inflammation in neurodegeneration, Cell 140 (2010) 918−934.
[4] E. Perry, B. Tomlinson, G. Blessed, K. Bergmann, P. Gibson, R. Perry, Correlation of cholinergic abnormalities with senile plaques and mental test scores in senile dementia, Br. J. Pharmacol. 2 (1978) 1457−1459.
[5] M. Harel, G. Kleywegt, R. Ravelli, I. Silman, J. Sussman, Crystal structure of an acetylcholinesterase-fasciculin complex: interaction of a three-fingered toxin from snake venom with its target, Structure 3 (1995) 1355−1366.
[6] K. Kucukoglu, H. Gul, P. Taslimi, I. Gulcin, C. Supuran, Investigation of inhibitory properties of some hydrazone compounds on hCA I, hCA II and AChE enzymes, Bioorg. Chem. 86 (2019) 316−321.
[7] N. Inestrosa, M. Dinamarca, A. Alvarez, Amyloid-cholinesterase interactions. Implications for Alzheimer's disease, FEBS J. 275 (2008) 625−632.
[8] P. Masson, O. Lockridge, Butyrylcholinesterase for protection from organophosphorus poisons: catalytic complexities and hysteretic behavior, Arch. Biochem. Biophys. 494 (2010) 107−120.
[9] D. Praticò, Oxidative stress hypothesis in Alzheimer's disease: a reappraisal, Trends in Pharmacological Sciences, Trends Pharmacol. Sci. 29 (2008) 609−615.
[10] M.G. Savelieff, G. Nam, J. Kang, H.J. Lee, M. Lee, M.H. Lim, Development of multifunctional molecules as potential therapeutic candidates for Alzheimer's disease, Parkinson's disease, and amyotrophic lateral sclerosis in the last decade, Chem. Rev. 119 (2018) 1221−1322.
[11] F. van Muiswinkel, H. Kuiperij, The Nrf2-ARE Signalling pathway: promising drug target to combat oxidative stress in neurodegenerative disorders, Curr. Drug Targets - CNS Neurol. Disord. 4 (2005) 267−281.
[12] K.P. Kepp, Bioinorganic chemistry of Alzheimer's disease, Chem. Rev. 112 (2012) 5193−5239.
[13] V. Kenche, K. Barnham, Alzheimer's disease & metals: therapeutic opportunities, Br. J. Pharmacol. 163 (2011) 211−219.
[14] R. Himes, G. Park, G. Siluvai, N. Blackburn, K. Karlin, Structural studies of copper(I) complexes of amyloid-beta peptide fragments: formation of two-coordinate bis(histidine) complexes, Angew. Chem. Int. Ed. Engl. 47 (2008) 9084−9087.
[15] M. Pohanka, Copper, aluminum, iron and calcium inhibit human acetylcholinesterase in vitro, Environ. Toxicol. Pharmacol. 37 (2014) 455−459.
[16] Y. Na, Recent cancer drug development with xanthone structures, J. Pharm. Pharmacol. 61 (2009) 707−712.
[17] F. Belluti, A. Rampa, L. Piazzi, A. Bisi, S. Gobbi, M. Bartolini, V. Andrisano, A. Cavalli, M. Recanatini, P. Valenti, Cholinesterase inhibitors: xanthostigmine derivatives blocking the acetylcholinesterase-induced beta-amyloid aggregation, J. Med. Chem. 48 (2005) 4444−4456.
[18] A. Contestabile, The history of the cholinergic hypothesis, Behav. Brain Res. 221 (2011) 334−340.
[19] M. Bolognesi, R. Banzi, M. Bartolini, A. Cavalli, A. Tarozzi, V. Andrisano, A. Minarini, M. Rosini, V. Tumiatti, C. Bergamini, R. Fato, G. Lenaz, P. Hrelia, A. Cattaneo, M. Recanatini, C. Melchiorre, Novel class of quinone-bearing polyamines as multi-target-directed ligands to combat Alzheimer's disease, J. Med. Chem. 50 (2007) 4882−4897.
[20] J. Liu, C. Zhang, H. Wang, L. Zhang, Z. Jiang, J. Zhang, Z. Liu, H. Chen, Incorporation of nitric oxide donor into 1,3-dioxyxanthones leads to synergistic anticancer activity, Eur. J. Med. Chem. 151 (2018) 158−172.
[21] G. Ellman, K. Courtney, V. Andres, R. Feather-Stone, A new and rapid colorimetric determination of acetylcholinesterase activity, Biochem. Pharmacol. 7 (1961) 88−95.

[22] M. Hoffmann, C. Stiller, E. Endres, M. Scheiner, S. Gunesch, C. Sotriffer, T. Maurice, M. Decker, Highly selective butyrylcholinesterase inhibitors with tunable duration of action by chemical modification of transferable carbamate units exhibit pronounced neuroprotective effect in an alzheimer's disease mouse model, J. Med. Chem. 62 (2019) 9116–9140.
[23] D. Bonda, X. Wang, G. Perry, A. Nunomura, M. Tabaton, X. Zhu, M. Smith, Oxidative stress in Alzheimer disease: a possibility for prevention, Neuropharmacology 59 (2010) 290–294.
[24] O.P. Sharma, T.K. Bhat, DPPH antioxidant assay revisited, Food Chem. 113 (2009) 1202–1205.
[25] N. Miller, C. Rice-Evans, Factors influencing the antioxidant activity determined by the ABTS.+ radical cation assay, Free Radic. Res. 26 (1997) 195–199.
[26] J. Jung, E. Lim, Y. Lee, J. Kang, H. Kim, S. Jang, S. Oh, M. Jung, Synthesis of novel trans-stilbene derivatives and evaluation of their potent antioxidant and neuroprotective effects, Eur. J. Med. Chem. 44 (2009) 3166–3174.
[27] Z. Wang, Y. Wang, W. Li, F. Mao, Y. Sun, L. Huang, X. Li, Design, synthesis, and evaluation of multitarget-directed selenium-containing clioquinol derivatives for the treatment of Alzheimer's disease, ACS Chem. Neurosci. 5 (2014) 952–962.
[28] S. Xie, J. Liu, C. Tang, C. Pang, Q. Li, Y. Qin, X. Nong, Z. Zhang, J. Guo, M. Cheng, W. Tang, N. Liang, N. Jiang, Design, synthesis and biological evaluation of rasagiline-clorgyline hybrids as novel dual inhibitors of monoamine oxidase-B and amyloid-β aggregation against Alzheimer's disease, Eur. J. Med. Chem. 202 (2020), 112475.
[29] Q. He, J. Liu, J. Lan, J. Ding, Y. Sun, Y. Fang, N. Jiang, Z. Yang, L. Sun, Y. Jin, S. Xie, Coumarin-dithiocarbamate hybrids as novel multitarget AChE and MAO-B inhibitors against Alzheimer's disease: design, synthesis and biological evaluation, Bioorg. Chem. 81 (2018) 512–528.
[30] L. Di, E.H. Kerns, K. Fan, O.J. McConnell, G.T. Carter, High throughput artificial membrane permeability assay for blood–brain barrier, Eur. J. Med. Chem. 38 (2003) 223–232.
[31] Y. Bourne, P. Taylor, Z. Radić, P. Marchot, Structural insights into ligand interactions at the acetylcholinesterase peripheral anionic site, EMBO J. 22 (2003) 1–12.
[32] Q. Li, S. Xing, Y. Chen, Q. Liao, B. Xiong, S. He, W. Lu, Y. Liu, H. Yang, Q. Li, F. Feng, W. Liu, Y. Chen, H. Sun, Discovery and biological evaluation of a novel highly potent selective butyrylcholinsterase inhibitor, J. Med. Chem. 63 (2020) 10030–10044.
[33] B. Kilic, H.O. Gulcan, F. Aksakal, T. Ercetin, N. Oruklu, E. Umit Bagriacik, D.S. Dogruer, Design and synthesis of some new carboxamide and propanamide derivatives bearing phenylpyridazine as a core ring and the investigation of their inhibitory potential on in-vitro acetylcholinesterase and butyrylcholinesterase, Bioorg. Chem. 79 (2018) 235–249.
[34] P. Sharma, A. Tripathi, P.N. Tripathi, S.S. Singh, S.P. Singh, S.K. Shrivastava, Novel molecular hybrids of N-benzylpiperidine and 1,3,4-oxadiazole as multitargeted therapeutics to treat Alzheimer's disease, ACS Chem. Neurosci. 10 (2019) 4361–4384.
[35] X. Zhang, G. Han, C. Guo, Z. Ma, M. Lin, Y. Wang, Z. Miao, W. Zhang, C. Sheng, J. Yao, Design, synthesis and biological evaluation of novel 3-hexyloxy chlorin e-based 15- or 13-amino acid derivatives as potent photosensitizers for photodynamic therapy, Eur. J. Med. Chem. 207 (2020), 112715.
[36] C. Lu, Y. Guo, J. Yan, Z. Luo, H. Luo, M. Yan, L. Huang, X. Li, Design, synthesis, and evaluation of multitarget-directed resveratrol derivatives for the treatment of Alzheimer's disease, J. Med. Chem. 56 (2013) 5843–5859.
[37] P. Cai, S. Fang, H. Yang, X. Yang, Q. Liu, L. Kong, X. Wang, Donepezil-butylated hydroxytoluene (BHT) hybrids as Anti-Alzheimer's disease agents with cholinergic, antioxidant, and neuroprotective properties, Eur. J. Med. Chem. 157 (2018) 161–176.
[38] Q. Liu, X. Qiang, Y. Li, Z. Sang, Y. Li, Z. Tan, Y. Deng, Design, synthesis and evaluation of chromone-2-carboxamido-alkylbenzylamines as multifunctional agents for the treatment of Alzheimer's disease, Bioorg. Med. Chem. 23 (2015) 911–923.
[39] L. Luo, Q. Song, Y. Li, Z. Cao, X. Qiang, Z. Tan, Y. Deng, Design, synthesis and evaluation of phthalide alkyl tertiary amine derivatives as promising acetylcholinesterase inhibitors with high potency and selectivity against Alzheimer's disease, Bioorg. Med. Chem. 28 (2020) 115400.
[40] D. Huang, B. Ou, M. Hampsch-Woodill, J. Flanagan, R. Prior, High-throughput assay of oxygen radical absorbance capacity (ORAC) using a multichannel liquid handling system coupled with a microplate fluorescence reader in 96-well format, J. Agric. Food Chem. 50 (2002) 4437–4444.